ELSEVIER

International Journal of Plasticity 20 (2004) 1139–1182

INTERNATIONAL JOURNAL OF Plasticity

www.elsevier.com/locate/ijplas

Analytical and experimental determination of the material intrinsic length scale of strain gradient plasticity theory from micro- and nano-indentation experiments

Rashid K. Abu Al-Rub, George Z. Voyiadjis*

Department of Civil and Environmental Engineering, Louisiana State University, Baton Rouge, LA 70803, USA

Received in final revised form 21 July 2003

Abstract

The enhanced gradient plasticity theories formulate a constitutive framework on the continuum level that is used to bridge the gap between the micromechanical plasticity and the classical continuum plasticity. They are successful in explaining the size effects encountered in many micro- and nano-advanced technologies due to the incorporation of an intrinsic material length parameter into the constitutive modeling. However, the full utility of the gradient-type theories hinges on one's ability to determine the intrinsic material length that scales with strain gradients, and this study aims at addressing and remedying this situation. Based on the Taylor's hardening law, a micromechanical model that assesses a nonlinear coupling between the statistically stored dislocations (SSDs) and geometrically necessary dislocations (GNDs) is used here in order to derive an analytical form for the deformation-gradient-related intrinsic length-scale parameter in terms of measurable microstructural physical parameters. This work also presents a method for identifying the length-scale parameter from micro- and nano-indentation experiments using both spherical and pyramidal indenters. The deviation of the Nix and Gao [Mech. Phys. Solids 46 (1998) 411] and Swadener et al. [J. Mech. Phys. Solids 50 (2002) 681; Scr. Mater. 47 (2002) 343] indentation size effect (ISE) models' predictions from hardness results at small depths for the case of conical indenters and at small diameters for the case of spherical indenters, respectively, is largely corrected by incorporating an interaction coefficient that compensates for the proper coupling between the SSDs and GNDs during indentation. Experimental results are also presented which show that the ISE for pyramidal and spherical indenters can be correlated successfully by using the proposed model.

Keywords: Gradient plasticity; Length scale; Indentation size effect

* Corresponding author. Tel.: +1-225-578-8668; fax: +1-225-578-9176.
E-mail address: voyiadjis@eng.lsu.edu (G.Z. Voyiadjis).

0749-6419/$ - see front matter © 2003 Elsevier Ltd. All rights reserved.
doi:10.1016/j.ijplas.2003.10.007

1. Introduction

Material length scales or size effects (i.e. the dependence of mechanical response on the structure size) have been of great importance in many engineering applications. Experimental work on particle-reinforced composites has revealed that a substantial increase in the macroscopic flow stress can be achieved by decreasing the particle size while keeping the volume fraction constant (Lloyd, 1994; Rhee et al., 1994a,b; Zhu and Zbib, 1995; Nan and Clarke, 1996; Kiser et al., 1996; Zhu et al., 1997). A similar strengthening effect associated with decreasing the diameter of thin wires in a micro-torsion test and thickness of thin beams in a micro-bending test has been reported by Fleck et al. (1994) and Stolken and Evans (1998), respectively. Moreover, micro- and nano-indentation tests have shown that the material hardness increases with decreasing indentation size (Stelmashenko et al., 1993; DeGuzman et al., 1993; Ma and Clarke, 1995; Poole et al., 1996; McElhaney et al., 1998; Lim and Chaudhri, 1999; Elmustafa and Stone, 2002, 2003; Swadener et al., 2002a,b). Indentation of thin films shows an increase in the yield stress with decreasing the film thickness (Huber et al., 2002). Experimental and numerical studies show an increase in the flow stress with decreasing hole size for geometrically similar perforated plates under tension, i.e. plates with a hole or several holes (e.g. Imamura and Sato, 1986; Taylor et al., 2002; Tsagrakis and Aifantis, 2002). Furthermore, there are many other well-known problems that show strong size effects. Example of which is testing of polycrystalline materials shows an increase in both yield and flow stresses, or equivalently the hardness, with decreasing the grain diameter; the so-called Hall–Petch behavior. Other similar effects are depicted when the fracture toughness K_{IC} in fracture design codes decreases with increasing thickness, the size of the process zone ahead of a crack tip decreases with increasing yield stress, increase in strength with decreasing the size of the notch for U-notched geometrically similar tensile bars, etc. These experiments have thus shown increasing in strength with decreasing size at the micron and submicron scales. The mechanical properties, such as flow stress or hardness, in metallic materials whether in simple tension, torsion, bending, or indentation testing are thus size dependent. In all of these cases, the representative length scale ℓ of the deformation field sets the qualitative and quantitative behavior of size effects. The classical continuum plasticity theory (Hill, 1950) cannot predict this size dependency since it does not possess an intrinsic material length-scale. On the other hand, it is still not possible to perform quantum and atomistic simulations on realistic time scale and structures. A multi-scale continuum theory, therefore, is needed to bridge the gap between the classical continuum theories and molecular dynamic simulations. In all of the problems mentioned above, a continuum approach is appropriate since the collective nature of material defects is sufficiently large and faraway from individuality.

In the last 10 years a number of authors have physically argued that the size dependence of the material mechanical properties results from an increase in strain gradients inherent in small localized zones which lead to geometrically necessary dislocations that cause additional hardening (e.g. Stelmashenko et al., 1993; DeGuzman et al., 1993; Fleck et al., 1994; Ma and Clarke, 1995; Arsenlis and Parks,

1999; Busso et al., 2000; Gao and Huang, 2003). Material deformation in metals enhances the dislocation formation, the dislocation motion, and the dislocation storage. The dislocation storage causes material hardening. The stored dislocations generated by trapping each other in a random way are referred to as statistically-stored dislocations (SSDs), while the stored dislocations that relieve the plastic deformation incompatibilities within the polycrystal caused by non-uniform dislocation slip are called geometrically-necessary dislocations (GNDs). Their presence causes additional storage of defects and increases the deformation resistance by acting as obstacles to the SSDs (Gao et al., 1999b). SSDs are believed to be dependent on the effective plastic strain, while the density of GNDs is directly proportional to the gradient of the effective plastic strain (Kroner, 1962; Ashby, 1970; Fleck and Hutchinson, 1997; Arsenlis and Parks, 1999). Accordingly, the theories of strain gradient plasticity have been proposed based on the concept of geometrically necessary dislocations in order to characterize the size effects. The smaller the length-scale, the larger the density of GNDs relative to the SSDs and, consequently, the larger the plastic strain gradients as compared to the average plastic strains. However, this area of study is still full of controversy and further experimental studies are needed.

Inspired by the aforementioned size effect problems, a number of gradient-enhanced theories have been proposed to address these problems through the incorporation of intrinsic length-scale measures in the constitutive equations, mostly based on continuum mechanics concepts. Gradient approaches typically retain terms in the constitutive equations of higher-order gradients with coefficients that represent length-scale measures of the deformation microstructure associated with the non-local continuum. Aifantis (1984) was one of the first to study the gradient regularization in solid mechanics. The gradient methods suggested by Lasry and Belytschko (1988) and Mühlhaus and Aifantis (1991) provide an alternative approach to the non-local integral equations (Kroner, 1967; Eringen and Edelen, 1972; Pijaudier-Cabot and Bazant, 1987). The gradient terms in several plasticity models are introduced through the yield function (e.g. Mühlhaus and Aifantis, 1991; de Borst and Mühlhaus, 1992; Gao et al., 1999a; Fleck and Hutchinson, 2001; Chen and Wang, 2002a). The gradient concept has been extended to the gradient damage theory that has been developed for isotropic damage (e.g. Peerlings et al., 1996) and for anisotropic damage (e.g. Kuhl et al., 2000; Voyiadjis et al., 2001; Voyiadjis and Dorgan, 2001). In addition, extension of the gradient theory to rate-dependent plasticity/damage has been made recently by few authors (Wang et al., 1998; Aifantis et al., 1999; Oka et al., 2000; Voyiadjis et al., 2003a,b; Gurtin, 2003; Saczuk et al., 2003). The gradient plasticity theories have given reasonable agreements with the aforementioned size dependence encountered in composite material experiments (e.g. Fleck and Hutchinson, 1997; Shu and Fleck, 1999; Shu and Barrlow, 2000; Busso et al., 2000; Bassani, 2001; Xue et al., 2002a), micro- and nano-indentation experiments (e.g. Nix and Gao, 1998; Shu and Fleck, 1998; Begley and Hutchinson, 1998; Gao et al., 1999b; Huang et al., 2000a,; Yuan and Chen, 2001) as well as with the micro-bend and micro-twist experiments (Gao et al., 1999b; Aifantis, 1999; Tsagrakis and Aifantis, 2002). There are also many gradient-enhanced models that

were proposed as a localization limiter, i.e. in order to avoid a spurious solution of the localization problem and excessive mesh dependence in conventional plasticity and damage (e.g. Aifantis, 1984, 1987; Lasry and Belytschko, 1988; de Borst et al., 1993; de Borst and Pamin, 1996; Bammann et al., 1999; Voyiadjis et al., 2001, 2003a,b; Voyiadjis and Dorgan, 2001).

Although there has been a tremendous theoretical work to understand the physical role of the gradient theory, this research area is still in its critical state with numerous controversies. This is due to some extent to the difficulty in calibration of the different material properties associated with the gradient-dependent models, which is impossible for certain cases. But more importantly is the difficulty of carrying out truly definitive experiments on critical aspects of the evolution of the dislocation patterns and crack and void structures. Furthermore, it is believed that the calibration of the constitutive coefficients of a gradient-dependent model should not only rely on stress–strain behavior obtained from macroscopic mechanical tests, but should also draw information from micromechanical, gradient-dominant tests such as micro/nano-indentation tests, micro-bending tests, and/or micro-torsion tests accompained by metallographic studies and stereology based quantification methods using tomography images. Thus, the full utility of gradient-based models hinges on one's ability to determine the constitutive length parameter that scales the gradient effects. The work reported here aims at addressing and remedying this situation.

At present, it appears that only micro- and nano-indentation hardness has been measured extensively by many experimentalists and found to exhibit strong size dependence as the depth of indentation approaches micron or sub-micron scale, while very limited experimental work has been conducted for studying the size effects encountered in micro-bending of thin beams and micro-torsion of thin wires. The study of Begley and Hutchinson (1998) indicated that indentation experiments may be the most effective test for measuring the length-scale parameter ℓ. The material properties of gradient theories cannot be effectively determined using a typical tension test where uniform deformation is encountered, while in indentation tests significant work hardening takes place due to severe and non-uniform plastic and damage deformation concentrated in the localized region directly below the indentation, outside of which the material still behaves elastically (Hill, 1950; Johnson, 1985). However, it appears that very few researchers have considered the identification of the material intrinsic length ℓ of gradient-enhanced theories from measurements of indentation tests. Begley and Hutchinson (1998) inferred ℓ from hardness experimental data for a number of materials and found ℓ to lie with the range of 0.25–1 μm, with the smallest values for the hardest materials. Nix and Gao (1998) estimated the material length scale parameter ℓ from the micro-indentation experiments of McElhaney et al. (1998) to be 12 μm for annealed single crystal copper and 5.84 μm for cold worked polycrystalline copper. Yuan and Chen (2001) proposed that the unique intrinsic material length parameter ℓ can be computationally determined by fitting the Nix and Gao (1998) model from micro-indentation experiments and they have identified ℓ to be 6 μm for polycrystal copper and 20 μm for single crystal copper. There have also been some experimental efforts to

determine the material length ℓ by micro-torsion and micro-bending tests of thin specimens. Based on Fleck et al. (1994) micro-torsion test of thin copper wires and Stolken and Evans (1998) micro-bend test of thin nickel beams, the material length parameter is estimated to be 4 μm for copper and 5 μm for nickel. Aifantis and his co-workers gave an estimate for ℓ by fitting Fleck et al. (1994) and Stolken and Evans (1998) experiments as 3.9–4.9 μm for copper and 6.5–15.6 μm for nickel. Furthermore, Wang et al. (2003) presented a theoretical analysis of different micro-bend test specimens in order to show their suitability for the determination of intrinsic material length in strain gradient plasticity theory. Their analysis confirms the findings of Stolken and Evans (1998).

In considering the microstructure with localization zones, the gradient-dependent behavior is expected to become important once the length-scale associated with the local deformation gradients become sufficiently large as compared with the controlling microstructural feature (e.g. mean spacing between inclusions relative to the inclusion size when considering a microstructure with dispersed inclusions, size of the plastic process zone at the front of the crack tip, the mean spacing between dislocations, the grain size and/or grain boundary thickness in polycrystalline materials, etc.). Thus, one major issue in strain-gradient plasticity is the determination of the intrinsic material length that scales with strain gradients. Recently, Voyiadjis et al. (2003a,b) developed a general thermodynamic framework for the analysis of heterogeneous media that assesses a strong coupling between rate-dependent plasticity and anisotropic rate-dependent damage. They showed that the variety of plasticity and damage phenomena at small-scale level dictates the necessity of more than one length parameter in the gradient description. They tend to express these material length measures in terms of macroscopic measurable material parameters. Similar phenomenological expressions have been assumed by Aifantis and co-authors (Konstantinidis and Aifantis, 2002; Tsagrakis and Aifantis, 2002). Nevertheless, an initial attempt has been made recently to relate ℓ to the micro-structure of a material. Based on the Taylor model in dislocation mechanics, Nix and Gao (1998) identified ℓ as L_S^2/b, where L_S is the average spacing between SSDs at plastic yield, and b is the modulus of the Burgers vector. Abu Al-Rub and Voyiadjis (in press) found ℓ to be proportional to L_S and derived an evolution equation for ℓ as a function of temperature and strain-rate. The work presented here is a continuation of Abu Al-Rub and Voyiadjis (in press) paper and focuses on identifying the material intrinsic length parameter ℓ in plasticity gradient theories through establishing a bridge between the plasticity at the micromechanical scale with the plasticity at the macromechanical scale. A constitutive framework is formulated using a micromechanical model that assesses a nonlinear coupling between statistically stored dislocation and geometrically necessary dislocation densities. The employed micromechanical model, which is based on the Taylor's hardening law, is used to link the strain-gradient effect at the microscopic scale with the stress-strain behavior of an equivalent continuum with homogenized plastic deformation at the macroscopic level. This constitutive framework yields expressions for the deformation-gradient-related intrinsic length-scale parameter ℓ in terms of measurable microstructural physical parameters.

Moreover, we present here a method for identifying the material intrinsic length parameter from micro and nano-indentation tests using both spherical and pyramidal (e.g. Berkovich and Vickers) indenters. However, despite the fact that the indentation size effect (ISE) has been reported by many well-reputed experimental groups, there are still points of controversy in addressing this type of size effects. This study also shed some insight on interpretation of the ISE encountered in micro- and nano-hardness results from spherical and pyramidal indenters. By considering the GNDs generated by a conical indenter, Nix and Gao (1998) developed a relation that suggests a linear dependence of the square of the micro-hardness to the inverse of the indentation depth. Swadener et al. (2002a,b) utilized the basic precepts given by Nix and Gao (1998) for a conical indenter and developed an ISE model for spherical indenters which suggests a linear dependence of the square of the micro-hardness to the inverse of the diameter of the indenter. Therefore, Nix and Gao (1998) interpreted the ISE as an increase in the hardness values with decreasing in the depth of indentation, while Swadener et al. (2002a) showed a dependence of hardness on the diameter of the indenter rather than on the depth of indentation. This controversy in interpreting the ISE is successfully explained in this work. Furthermore, recent micro- and nano-indentation results show that the Nix and Gao and Swadener et al. models predictions deviate from the experimental results at small depths in the case of Berkovich and Vickers indenters (Lim and Chaudhri, 1999; Saha et al., 2001) and at small diameters for the case of spherical indenters (Swadener et al., 2002a). Modification of the Nix and Gao and Swadener et al. models is proposed in this study in order to solve this deviation.

Finally, by combining indentation size effect relations developed for both spherical and pyramidal indenters, we find a correlation between the measured hardness from both indenter geometries. This correlation is corroborated by previous experiments on iridium (Swadener et al., 2002a) and oxygen free copper (Lim et al., 1998; Lim and Chaudri, 1999).

2. Analytical determination of the plasticity length-scale

2.1. Hardening at the macroscopic scale

Many researchers tend to write the weak form of the non-local conventional effective plastic strain ($\widehat{p}$), the conjugate variable of the plasticity isotropic hardening, in terms of its local counterpart (p) and corresponding high-order gradients (η). However, the coupling between p and η was presented in many different mathematical forms. The following modular generalization of p can be defined as follows:

$$\widehat{p} = [f(p)^{\gamma_1} + g(\ell\eta)^{\gamma_2}]^{1/\gamma_3} \tag{1}$$

where ℓ is a length parameter that is required for dimensional consistency and whose role will be examined in detail later in this paper. f is a function of the effective plastic strain p and $g(\ell\eta)$ is the measure of the effective plastic strain gradient of any order. The superimposed hat denotes the spatial non-local operator. γ_1, γ_2, and γ_3

are phenomenological material constants, termed here as *interaction coefficients*, which are introduced in order to assess the sensitivity of the predictions to the way in which p and η are coupled. The work of Aifantis and his co-authors (see for example Aifantis, 1984, 1987; Zbib and Aifantis, 1988; Mühlhaus and Aifantis, 1991 and references quoted therein) falls within $\gamma_1 = \gamma_2 = \gamma_3 = 1$. Two distinct expressions for the gradient term η were proposed by Aifantis and his co-workers: $\ell\eta = \ell||\nabla p|| = \ell\sqrt{\nabla p.\nabla p}$ and $\ell\eta = \ell^* \nabla^2 p$ with $\ell = \sqrt{\ell^*}$, where ∇ and ∇^2 are, respectively, the forward gradient and Laplacian operators. The latter form has been used by de Borst and his co-workers and by many others in solving the localization problem (see for example de Borst and Mühlhaus, 1992; de Borst et al., 1993; de Borst and Pamin, 1996; and references quoted therein).

A different strain-gradient plasticity theory of Cosserat type has been introduced by Fleck and co-workers (see for example Fleck et al., 1994; Fleck and Hutchinson, 1993, 1997, 2001; and references quoted therein). This type of strain-gradient theory falls within $\gamma_1 = \gamma_2 = \gamma_3 = 2$ with $\ell\eta$ expressed as $\ell\eta = c_1\eta_{iik}\eta_{jjk} + c_2\eta_{ijk}\eta_{ijk} + c_3\eta_{ijk}\eta_{kji}$, where c_n ($n = 1,\ldots,3$) are material coefficients of length-square dimension. The third-order tensor $\boldsymbol{\eta}$ is defined as the second gradient of displacement $\boldsymbol{u}$, such that $\eta = \nabla\nabla\boldsymbol{u}$, or alternatively defined as the first gradient of the plastic strain ε^{p}, such that $\boldsymbol{\eta} = \nabla\varepsilon^{\mathrm{p}}$. The mechanism-based strain-gradient (MSG) plasticity theory and the Taylor-based nonlocal theory (TNT) of plasticity by Gao and his co-workers, which are based on the work of Fleck and his co-workers, correspond to the case of $\gamma_1 = \gamma_3 = 2$ and $\gamma_2 = 1$ (see for example Nix and Gao, 1998; Gao et al., 1999a; Huang et al., 2000a; Gao and Huang, 2001; Hwang et al., 2002; and references quoted therein). Those types of strain-gradient theories have been used by many authors to solve the problem of size effects encountered in a variety of problems of mechanical behavior at small scales, including the strengthening of twisted wires of reducing diameter, the strengthening of bended beams of reducing thickness, particle reinforced composites, microelectromechanical systems (MEMS), indentation, crack tips, and void growth (see for example Begley and Hutchinson, 1998; Stolken and Evans, 1998; Saha et al., 2001; Gao et al., 1999a,b; Huang et al., 2000b; Gao and Huang, 2001; Guo et al., 2001; Chen and Wang, 2002b; Konstantinidis and Aifantis, 2002; Xue et al., 2002a,b,c; Wang et al., 2003; Hwang et al., 2003; and references quoted therein).

However, for simplicity, we will assume in the subsequence of this paper that $f(p) = p$, $g(\ell\eta) = \ell\eta$, and $\gamma_1 = \gamma_2 = \gamma_3 = \gamma$ (Fleck and Hutchinson, 1997; Begley and Hutchinson, 1998), such that $\bar{p}$ can be expressed as follows:

$$\bar{p} = [p^{\gamma} + (\ell\eta)^{\gamma}]^{1/\gamma} \tag{2}$$

where γ is an interaction coefficient. Eq. (2) ensures that $\bar{p} \to p$ whenever $p >> \ell\eta$ and that $\bar{p} \to \ell\eta$ whenever $p << \ell\eta$. Two values of γ are generally investigated in the literature: (1) $\gamma = 1$ which corresponds to a superposition of the contributions of the local plastic strain and the higher-order gradients of the plastic strain to the flow stress; and (2) $\gamma = 2$ which, since the effective plastic strain scales with the norm of the plastic strain tensor, corresponds to a superposition of the effective plastic strain of the two types of local and non-local parts.

The homogenous flow stress σ_f without the effect of deformation gradients can be identified, in general, as follows (e.g. Nix and Gao, 1998; Huang et al., 2000a,b; Yuan and Chen, 2001):

$$\sigma_f = \sigma_o f(p) \tag{3}$$

where σ_o is a measure of the yield stress in uniaxial tension. For the majority of ductile materials, the function f can be written as a power-law relation (e.g. Fleck and Hutchinson, 1997; Kucharski and Mroz, 2001; Hwang et al., 2002), such that:

$$f(p) = p^{1/m} \tag{4}$$

where $m \geqslant 1$ is the hardening exponent which can be determined from a simple uniaxial tension test or indentation test.

2.2. Hardening at the microscopic scale

The Taylor hardening law that relates the shear strength to the dislocation density has been the basis of the mechanism-based strain gradient (MSG) plasticity theory (e.g. Nix and Gao, 1998; Gao et al., 1999a; Huang et al., 2000a). It gives a simple description of the dislocation interaction processes at the microscale (i.e. over a scale which extends from about a fraction of a micron to tens of microns). One method to enhance the coupling between SSDs and GNDs is to assume that the overall shear flow stress, τ_f, has two components; one arising from SSDs, τ_S, and a component due to GNDs, τ_G. The following general functional form for τ_f is then chosen as follows in the spirit of Eq. (2) (Columbus and Grujicic, 2002):

$$\tau_f = \left[\tau_S^\beta + \tau_G^\beta\right]^{1/\beta} \tag{5}$$

where β is considered as a material constant, termed the *interaction coefficient*, and used to assess the sensitivity of predictions to the way in which the coupling between the SSDs and GNDs is enhanced during the plastic deformation process. τ_S and τ_G are given by the Taylor's hardening law as follows:

$$\tau_S = \alpha_S G b_S \sqrt{\rho_S} \tag{6}$$

$$\tau_G = \alpha_G G b_G \sqrt{\rho_G} \tag{7}$$

where b_S and b_G are the magnitudes of the Burgers vectors associated with SSDs and GNDs, respectively, and α_S and α_G are statistical coefficients which account for the deviation from regular spatial arrangements of the SSD and GND populations, respectively. For an impenetrable forest, it is reported that $\alpha_S \approx 0.85$ (Kocks, 1966) and $\alpha_G \approx 2.15$ (Busso et al., 2000).

This general form ensures that $\tau \to \tau_S$ whenever $\tau_S >> \tau_G$ and that $\tau \to \tau_G$ whenever $\tau_S << \tau_G$. Two values of β are generally investigated in the literature: (a) $\beta = 1$ which corresponds to a superposition of the contributions of SSDs and GNDs to the flow stress (e.g. Columbus and Grujicic, 2002); and (b) $\beta = 2$ which, since the

flow stress scales with the square root of dislocation density, corresponds to the superposition of the SSD and GND densities (e.g. Busso et al., 2000). Moreover, Eq. (5) constitutes the non-local micromechanical plasticity constitutive model due to the presence of GNDs. It is also imperative to emphasize that the validity of the Taylor relationship, Eqs. (6) or (7), has been verified by numerous theoretical and experimental studies (see e.g. Hirsch, 1975). Therefore, one may indeed use it as a starting point.

Expressing Eq. (5) in terms of Eqs. (6) and (7) yields a general expression for the overall flow stress in terms of SSD and GND densities, such that:

$$\tau_f = \alpha_S G b_S \left[\rho_S^{\beta/2} + \left(\frac{\alpha_G b_G}{\alpha_S b_S} \right)^{\beta} \rho_G^{\beta/2} \right]^{1/\beta} \tag{8}$$

Alternatively, Eq. (8) can be redefined in terms of an equivalent total dislocation density, ρ_T, as follows:

$$\rho_T = \left[\rho_S^{\beta/2} + \left(\frac{\alpha_G^2 b_G^2}{\alpha_S^2 b_S^2} \rho_G \right)^{\beta/2} \right]^{2/\beta} \tag{9}$$

so that

$$\tau_f = \alpha_S G b_S \sqrt{\rho_T} \tag{10}$$

Using the basic functional form of the Taylor relationship as shown by Eq. (10), one can devise different ways of coupling the SSD and GND densities under ρ_T; however, all are special cases of Eq. (9). For instance, many authors tend to write ρ_T as a linear sum of ρ_S and ρ_G, such that $\rho_T = \rho_S + \rho_G$ (e.g. Ashby, 1970; Stelmashenko et al., 1993; DeGuzman et al., 1993; Fleck et al., 1994; Ma and Clarke, 1995; Nix and Gao, 1998; etc). Eq. (9) reduces to this case when $\alpha_S = \alpha_G$, $b_S = b_G$, and $\beta = 2$. Another possible coupling between the SSD and GND densities has been proposed by Fleck and Hutchinson (1997), where they expressed ρ_T as the harmonic sum of ρ_S and ρ_G, such that $\rho_T = \sqrt{\rho_S^2 + \rho_G^2}$. Eq. (9) reduces to this case when $\alpha_S = \alpha_G$, $b_S = b_G$, and $\beta = 4$. Moreover, Kocks et al. (1975) proposed a general form as $\rho_T = \left[\rho_S^{\mu} + \rho_G^{\mu}\right]^{1/\mu}$. This can be obtained from Eq. (9) by setting $\alpha_S = \alpha_G$, $b_S = b_G$, and $\beta = 2\mu$. Thus, all the mentioned possibilities of coupling between SSDs and GNDs are special cases of the general form in Eq. (9).

The tensile flow stress σ_f is related to the shear flow strength through the Taylor factor Z, such that:

$$\sigma_f = Z\tau_f = Z\alpha_S G b_S \sqrt{\rho_T} \tag{11}$$

where σ_f is equivalent to the effective stress, and the Taylor factor Z acts as an isotropic interpretation of the crystalline anisotropy at the continuum level (Gao et al., 1999b); $Z = \sqrt{3}$ for an isotropic solid and $Z = 3.08$ for FCC polycrystalline metals (Taylor, 1938; Bishop and Hill, 1951; Kocks, 1970).

2.3. Bridging the gap between the macro- and micro-scale hardening

Generally, it is assumed that the total dislocation density, ρ_T, represents the total coupling between the two types of dislocations which play a significant role in the hardening mechanism. Material deformation enhances dislocation formation, dislocation motion, and dislocation storage. Dislocation storage causes material hardening. As was previously outlined, SSDs are generated by trapping each other in a random way, while GNDs are stored in order to maintain the deformation compatibility within the polycrystalline metal. The presence of GNDs causes additional storage of defects and increases the deformation resistance by acting as obstacles to the SSDs and mobile dislocations. The SSDs are created by homogenous strain and are related to the plastic strain, while the GNDs are related to the curvature of the crystal lattice or to the strain gradients (Kroener, 1962; Ashby, 1970). Plastic strain gradients appear either because of geometry of loading and boundary conditions or because of inhomogeneous deformation in the material. Hence, GNDs are required to account for the permanent shape change. The non-local effective plastic strain in Eq. (2) is intended to measure the total dislocation density that accounts for both: dislocations that are statistically stored and geometrically necessary dislocations induced by the strain gradients (Gao et al., 1999b, Fleck and Hutchinson, 2001).

However, since uniaxial tension tests exhibit homogenous deformation, Eq. (3) cannot be used to describe applications where the non-uniform plastic deformation plays an important role (e.g. twisting, bending, deformation of composites, micro- or nano-indentation, etc.). Eq. (3) cannot then predict the size dependence of material behavior after normalization, which involves no internal material length-scales. Consequently, Eq. (3) needs to be modified in order to be able to incorporate the size effects. This can be effectively done by replacing the conventional effective plastic strain measure p by its corresponding non-local measure $\widehat{p}$ defined by Eq. (2), such that we can consider a more general hardening relation:

$$\sigma_f = \sigma_o[p^\gamma + (l\eta)^\gamma]^{1/m\gamma} \tag{12}$$

where σ_f can also be set equal to the effective or equivalent stress $\sigma_{eff} = \sqrt{3\sigma'_{ij}\sigma'_{ij}/2}$ in case of the von-Mises type plasticity or $\sigma_{\text{eff}} = \sqrt{\sigma'_{ij}\sigma'_{ij}} + \alpha\sigma_{kk}$ in case of a Drucker–Prager plasticity (σ'_{ij} denotes the deviatoric component of the stress tensor σ_{ij}). The above strain gradient law exactly matches the Fleck–Hutchinson (1993) phenomenological law in the case of a single material length scale with γ taken to be 2, but can be generalized to any arbitrary number larger than 1 without destroying the basic theoretical framework (Fleck and Hutchinson, 1997).

It is imperative to note that the non-local effects associated with the presence of local deformation gradients at a given material point are incorporated into Eq. (11) through GND density (Busso et al., 2000). Thus, Eq. (11) constitutes the non-local micromechanical plasticity constitutive model. Moreover, at the microscale, where dislocation densities are used as the appropriate variables to describe plastic flow, the introduction of higher-order gradient terms in the conventional continuum mechanics [i.e. Eq. (12)] has led the bridging of the gap between conventional

continuum theories and micromechanical models. Eqs. (11) and (12) imply that plasticity is the macroscopic outcome from the combination of many dislocation elementary properties at the micro and mesoscopic scale. These two equations, therefore, represent the link of microscale plasticity to the macroscopic plasticity. The effective use of this link will be demonstrated in what follows.

Arsenlis and Parks (1999), Gao et al. (1999a,b), and Huang et al. (2000a) showed that gradients in the plastic strain field are accommodated by the GND density, ρ_G, so that the effective strain gradient η that appears in Eq. (12) can be defined as follows:

$$\eta = \frac{\rho_G b_G}{\bar{r}} \tag{13}$$

They showed that this expression allows η to be interpreted as the deformation curvature in bending and the twist per unit length in torsion. $\bar{r}$ is the Nye factor introduced by Arsenlis and Parks (1999) to reflect the scalar measure of GND density resultant from macroscopic plastic strain gradients. For FCC polycrystals, Arsenlis and Parks (1999) have reported that the Nye factor has a value of $\bar{r} = 1.85$ in bending and a value of $\bar{r} = 1.93$ in torsion. The Nye factor is an important parameter in the predictions of the gradient plasticity theories as compared to the experimental results (Gao et al., 1999b).

With the aid of Eq. (12), which expresses the flow stress in the macroscale, along with the Taylor's hardening law, Eq. (11), in the microscale, one can derive an analytical expression for the material intrinsic length ℓ for isotropic hardening gradient plasticity as a function of physical microstructural parameters. However, in order to do that a relation between the effective plastic strain (p) and the density of SSDs is required. During plastic deformation, the density of SSDs increases due to a wide range of processes that lead to production of new dislocations. Those new generated dislocations travel on a background of GNDs which act as obstacles to the SSDs. If L_S is the average distance traveled by a newly generated dislocation, then the rate of accumulation of strain due to SSDs scales with $\dot{p} \propto L_S b_S \dot{\rho}_S$. Bammann and Aifantis (1982) defined the plastic shear strain, γ^{p}, as a function of the mobile dislocation density. However, a similar relation can then be assumed for the evolution of ρ_S in terms of γ^{p} for proportional loading (Abu Al-Rub and Voyiadjis, in press), such that:

$$\gamma^{\mathrm{p}} = b_S L_S \rho_S \tag{14}$$

where L_S is the mean spacing between SSDs. Furthermore, Bammann and Aifantis (1982) generalized the plastic strain in the macroscopic plasticity theory, $\boldsymbol{\varepsilon}^{\mathrm{p}}$, in terms of the plastic shear strain, γ^{p}, and an orientation tensor, $\boldsymbol{M}$, as follows:

$$\varepsilon^{\mathrm{p}}_{ij} = \gamma^{\mathrm{p}} M_{ij} \tag{15}$$

where M is the symmetric Schmidt's orientation second-order tensor. In expressing the plastic strain tensor at the macro level to the plastic shear strain at the micro level, an average form of the Schmidt's tensor is assumed since plasticity at the macroscale incorporates a number of differently oriented grains into each

continuum point (Bamman and Aifantis, 1982, 1987). Moreover, average values are used for the magnitude of the Burgers vector, $\boldsymbol{b}_S$, and the mean spacing between SSDs, L_S.

The flow stress σ_f is the conjugate of the effective plastic strain variable p in macro-plasticity. For proportional, monotonically increasing plasticity, p is defined as:

$$p = \sqrt{\frac{2}{3}\boldsymbol{\varepsilon}^{\mathrm{p}}_{ij}\boldsymbol{\varepsilon}^{\mathrm{p}}_{ij}} \tag{16}$$

Hence, utilizing Eqs. (14) and (15) into Eq. (16), one can write p as a function of SSDs as follows:

$$p = b_S L_S \rho_S \bar{M} \tag{17}$$

which is referred to as the Orowan-like equation (Abu Al-Rub and Voyiadjis, in press), where $\bar{M} = \sqrt{2\boldsymbol{M} : \boldsymbol{M}/3}$ can be interpreted as the Schmidt's orientation factor. It is clear from Eq. (17) that the Burgers vector and the dislocation spacing are two physical length measures which control plastic deformation.

Substituting ρ_G and ρ_S from Eqs. (13) and (17), respectively, into Eq. (11), yields the following expression for the flow stress σ_f:

$$\sigma_f = Z\alpha_S G\sqrt{\frac{b_S}{L_S\bar{M}}}\left[p^{\beta/2} + \left(\frac{\alpha_G^2 b_G L_s \bar{M}\,\bar{r}}{\alpha_S^2 b_S}\eta\right)^{\beta/2}\right]^{1/\beta} \tag{18}$$

Comparing Eq. (18) with Eq. (12) yields the following relations:

$$\gamma = \beta/2, \quad m = 2, \quad \sigma_o = Z\alpha_S G\sqrt{\frac{b_S}{L_S\bar{M}}} \tag{19}$$

with the intrinsic material length-scale ℓ expressed as follows:

$$\ell = \hbar L_S \quad \text{where} \quad \hbar = (\alpha_G/\alpha_S)^2(b_G/b_S)\bar{M}\bar{r} \tag{20}$$

The phenomenological measure of the yield stress in uniaxial tension, σ_o, and the microstructure length-scale parameter, ℓ, are now related to measurable physical parameters. Therefore, the form and magnitude of ℓ depend on the dominant mechanism of plastic flow at the scale under consideration. It appears from Eq. $(20)_1$ that the size effect and its implications on the flow stress and work-hardening is fundamentally controlled by dislocation glide. Also, the mapping between micro and macro plasticity results in $\gamma = \beta/2$, which is rational for the following reason. One possible coupling between ρ_S and ρ_G was presented as $\rho_T = \rho_S + \rho_G$ with $\beta = 2$, and that ρ_G and ρ_S are linear in the gradient of the plastic strain [Eq. (13)] and the plastic strain [Eq. (14)], respectively. One concludes then that an appropriate scalar

measure of hardening is given by Eq. (2) with $\gamma = \beta/2 = 1$. Moreover, another possible coupling between ρ_S and ρ_G can be expressed as $\rho_T^2 = \rho_S^2 + \rho_G^2$ with ρ_S and ρ_G are obtained from Eqs. (14) and (13), respectively. Hence, one concludes that the hardening law [Eq. (12)] is appropriately expressed with $\gamma = \beta/2 = 2$. Furthermore, the condition $m = 2$ is not unreasonable for some materials (Nix and Gao, 1998), particularly for some annealed crystalline solids. However, the authors believe that the origin of this condition, as it is concluded from the mathematical setup of Eqs. (11) and (12), comes out from the assumption that the Taylor's flow stress is directly proportional to the square root of the dislocations density (i.e. $\tau_f \propto \sqrt{b^2\rho_T}$), which can be rewritten as $\rho_T^{1/m}$ with $m = 2$. More generally, one can assume that $\tau_f \propto \left(b^2\rho_T\right)^{1/m}$ with $m \geqslant 1$. This is not the subject of this work, but further study needs to be carried out to show the importance of this generalization.

Moreover, by substituting $L_S\bar{M}$ from Eq. $(19)_3$ into Eq. (20) one obtains a relation for ℓ as a function of the shear modulus and yield stress, such that:

$$\ell = Z^2\alpha_G^2 b_G \bar{r}\left(\frac{G}{\sigma_o}\right)^2 \tag{21}$$

It is imperative to mention that based on the Taylor relationship, Nix and Gao (1998) have identified ℓ as the square of SSD spacing over the Burgers vector, i.e. $\ell = L_S^2/b$, which shows that the length scale is proportional L_S as appears in Eq. (20). Therefore, L_S is the main physical measure that controls the evolution of the length scale in gradient plasticity theory. In terms of the macroscopic quantities, this length scale was given as $\ell = b\left(G/\sigma_f\right)^2$, which is similar to Eq. (21). Moreover, one can note that Eq. (21) implies that the length-scale parameter may vary with the strain-rate and temperature for a given material for the case $\sigma_o = \sigma_o(\dot{p}, T)$, where $\dot{p} = \sqrt{2\dot{\varepsilon}_{ij}^{\mathrm{p}}\dot{\varepsilon}_{ij}^{\mathrm{p}}/3}$. However, for most metals, the yield stress increases with the strain rate and decreases with temperature increase. This causes ℓ to decrease with increasing strain-rates, but to increase with temperature decrease (Abu Al-Rub and Voyiadjis, in press).

3. Identification of the length-scale from hardness experiments

It is well-known by now that the micro- or nano-indentation hardness of metallic materials displays strong size effect. Indentation tests at scales on the order of a micron or a submicron have shown that measured hardness increases significantly with decreasing indent size. This has been attributed to the evolution of geometrically necessary dislocations associated with gradients. Next we present a simple procedure to identify the intrinsic material length parameter that scales the effect of GNDs using both spherical and pyramidal (Berkovich and Vickers) indenters.

Tabor (1951) and Atkins and Tabor (1965) showed in their experiments that the elasto-plastic material response in tensile testing could be correlated to the response in spherical (or Brinell) indentation. The fundamental parameters for indentation tests are: the force applied to the indenter P, the residual contact radius of indentation a_p,

the contact pressure (hardness) $H = P/\pi a_p^2$, the permanent indentation depth h_p, the total indentation depth h, the residual indentation profile diameter D_p, and the indenter geometry (i.e. the sphere diameter D). The unloading process in the indentation experiment is most important for the proper specification of these geometric parameters. Thus, h_p and a_p should be used as measurable data in the hardness H calculation as well as the residual indentation profile diameter $D_p > D$ when using spherical indenters.

Consider now the indentation by a rigid sphere, as shown schematically in Fig. 1. We assume that the density of geometrically necessary dislocations is integrated by the geometry of the indenter and the indentation is accommodated by circular loops of GNDs with Burgers vectors normal to the plane of the surface. We also assume that the densities of statistically stored dislocations and geometrically necessary dislocations are coupled as proposed by Eq. (9). One can use the simple model of GNDs developed by Stelmashenko et al. (1993), DeGuzman et al. (1993), Nix and Gao (1998), and Swadener et al. (2002a,b) to determine the density of GNDs evolved under a spherical indenter. The present development follows to some extent the approach of Nix and Gao (1998) and Swadener et al. (2002a,b). As the spherical indenter is forced into the surface of a single crystal, GNDs are required to account

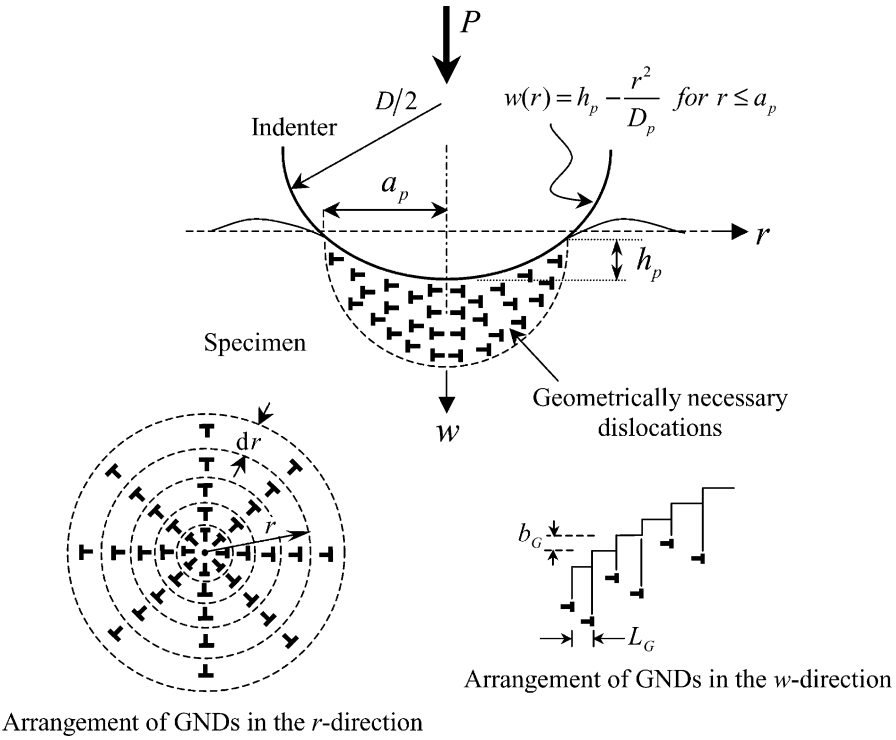

Fig. 1. Axisymmetric rigid spherical indenter. Geometrically necessary dislocations created during the indentation process. The dislocation structure is idealized as circular dislocation loops.

for the permanent shape change at the surface. Of course SSDs, not shown in Fig. 1, would also be created and they would contribute to the deformation resistance.

In early hardness experiments, it was concluded that the relation between the hardness, H, and the permanent indentation depth, h_p, follows a power law. Making use of this observation, Tabor (1951) specified the mapping from the hardness–indentation depth curve ($H-h$ curve) to the tensile stress–plastic strain curve ($\sigma-p$), such that one can assume the following:

$$H=\kappa\sigma_f \quad p=c\left(\frac{a_p}{D_p}\right) \tag{22}$$

where κ is the Tabor's factor of $\kappa=2.8$ and c is a material constant with a value of $c=0.4$ (Atkins and Tabor, 1965), while corresponding numerical results from Biwa and Storakers (1995) are: $\kappa=3.07$ and $c=0.32$. More generally a value between a $c=0.342$ to 0.376 has been determined by Johnson (1985) for a strain-hardening coefficient from $m=1$ to infinity. The relations in Eq. (22) were used by many authors (e.g. Robinson and Truman, 1977; Tangena and Hurkx, 1986; Oliver and Pharr, 1992; Huber and Tsakmakis, 1999; Kucharski and Mroz, 2001; Caceres and Poole, 2002) for determining the stress–strain response on the basis of spherical indentation tests. However, it should be remarked that the above reported numerical values for κ and c are appropriate only for work-hardened ductile materials and for relatively large indentation depths (Lim and Chaudhri, 1999). Over the last 10 years, the Tabor's Eqs. (22) are strongly taken into reconsideration (see e.g. Shen and Chawla, 2001; Caceres and Pool, 2002, and the references quoted therein). Nevertheless, one may take them as a starting point.

It can be assumed that the spherical indenter is approximated by a paraboloid, and the indentation profile in the unloaded configuration can be described by (e.g. Biwa and Storakers, 1995; Kucharski and Mroz, 2001):

$$w(r)=h_p-\frac{r^2}{D_p} \quad \text{for} \quad 0\leqslant r\leqslant a_p \tag{23}$$

where h_p, a_p, and D_p are measured in the unloaded configuration, which are characterized as the residual values after unloading. By taking the slope of Eq. (23) and comparing it with Fig. 1, one can easily show that:

$$\left|\frac{\mathrm{d}w}{\mathrm{d}r}\right|=\frac{2r}{D_p}=\frac{b_G}{L_G} \quad \text{or} \quad L_G=\frac{b_G D_p}{2r} \tag{24}$$

where L_G is the mean spacing between individual slip steps on the indentation surface corresponding to the GND loops. Note that the individual dislocation loops of GNDs are being unequally spaced along the surface of the indentation. The dislocation loops are closely spaced near to the indenter tip and the spacing between them increases as one moves faraway from the tip of the indenter (i.e. $L_G\propto 1/r$). This agrees well with the experimental observations made by Chiu and Ngan (2002) who reported that the nucleation and evolution of GNDs are maximum at the tip of

the indenter. If λ is the total length of the injected loops, then between r and $r+\mathrm{d}r$ we have:

$$\mathrm{d}\lambda = 2\pi r \frac{\mathrm{d}r}{L_G} = 4\pi \frac{r^2}{b_G D_p}\mathrm{d}r \tag{25}$$

which after integration gives

$$\lambda = \int_o^{a_p} \frac{4\pi}{b_G D_p} r^2 \mathrm{d}r = \frac{4\pi a_p^3}{3 b_G D_p} \tag{26}$$

Moreover, the dislocation evolution during indentation is primarily governed by a large hemispherical volume V defined by the contact radius a_p around the indentation profile. One can then assume that all the injected loops remain within the hemispherical volume V, such that:

$$V = \frac{2}{3}\pi a_p^3 \tag{27}$$

so that the density of geometrically necessary dislocations becomes

$$\rho_G = \frac{\lambda}{V} = \frac{2}{b_G D_p} \tag{28}$$

This relation shows that ρ_G underneath the spherical indenter is not a function of the indentation depth h (or equivalently the contact radius), contrary to that of a sharp, conical indenter. This confirms the recent find by Swadener et al. (2002a) and Gerberich et al. (2002).

Now considering the results derived in Section 2, the substitution of Eq. (18) into Eq. $(22)_1$, yields the following expression for hardness (H), such that:

$$H = Z\kappa\alpha_S G b_S \left[\rho_S^{\beta/2} + \left(\frac{\alpha_G b_G}{\alpha_S b_S}\right)^{\beta} \rho_G^{\beta/2}\right]^{1/\beta} \tag{29}$$

Moreover, one can define the macro-hardness H_o as the hardness that would arise from SSDs alone in the absence of strain gradients, such that (Nix and Gao, 1998):

$$H_o = Z\kappa\tau_S = Z\kappa\alpha_S G b_S \sqrt{\rho_S} \tag{30}$$

By dividing Eq. (29) by Eq. (30), one obtains the following relation:

$$\left(\frac{H}{H_o}\right)^{\beta} = 1 + \left(\frac{\alpha_G b_G}{\alpha_S b_S}\right)^{\beta} \left(\frac{\rho_G}{\rho_S}\right)^{\beta/2} \tag{31}$$

The density of SSDs (ρ_S) can be obtained by substituting Eqs. $(22)_2$ and (20) into Eq. (17), such that:

$$\rho_S = \frac{c\bar{r}\alpha_G^2 b_G a_p}{\ell b_S^2 \alpha_S^2 D_p} \tag{32}$$

Making use of Eqs. (28) and (32) into Eq. (31), one can now write the micro-hardness for spherical indenters as follows:

$$\left(\frac{H}{H_o}\right)^{\beta} = 1 + \left(\frac{a^*}{a_p}\right)^{\beta/2} \tag{33}$$

where a^* is given as:

$$a^* = \varsigma\ell \quad \text{with} \quad \varsigma = \frac{2}{c\bar{r}} \tag{34}$$

Substituting Eq. (32) into Eq. (30) along with Eq. (21), one can obtain a simple relation to predict the macro-hardness H_o as follows:

$$H_o = \kappa\sigma_o\sqrt{\frac{ca_p}{D_p}} \tag{35}$$

The above equation matches to a large extent the hardness expression (the Meyer hardness, Tabor, 1996) proposed first by Hill et al. (1989), and modified later by Field and Swain (1993), Adler and Dogan (1997), and Kucharski and Mroz (2001). Hill et al. (1989) provided a complete analysis of the sphere indentation problem for a non-linear elastic material satisfying the power law $\sigma = \sigma_o\varepsilon^{1/m}$, where ε is the total strain, and demonstrated that the relation between hardness and contact radius is of the form:

$$H_o = \kappa c^{1/m}\sigma_o\left(\frac{a_p}{D_p}\right)^{1/m} \tag{36}$$

Eq. (36) reduces to Eq. (35) when $m = 2$. A correction of Eq. (36) for elastic–plastic spherical indentation problem (i.e. materials satisfying the power-hardening law $\sigma = \sigma_o p^{1/m}$) was proposed by Field and Swain (1993), where they measured the contact radius a_p in Eq. (36) at the level of the undeformed surface. A different correction was provided by Adler and Dogan (1997) in order to account for variation of the indentation curvature during unloading, where D_p in Eq. (36) was specified in the unloaded configuration and the variation of a_p was neglected. However, Kucharski and Mroz (2001) considered the measurement of both a_p and D_p in the unloaded configuration. Moreover, Eq. (36) is usually used to identify the material parameters σ_o and m by measuring the variation of H_o with respect to a_p. Using a $\log(H_o) - \log(a_p/D_p)$ plot of Eq. (36), a linear diagram is obtained and its slope specifies the value of $1/m$ and its intercept is $\log(\kappa c^{1/m}\sigma_o)$.

3.1. Interpretation of the indentation size effect

It can be noted that both Eqs. (33) and (36) in addition to $H = P/\pi a_p^2$ are functions of the residual contact radius, a_p. Therefore, Eq. (33) cannot be used alone to characterize the indentation size effect (ISE) noticed in hardness experiments with spherical indenters. However, Lim and Chaudhri (1999), Tymiak et al. (2001), and Swadener et al. (2002a) have shown experimentally that for indentation of material with spherical indenters of few microns tip radii, the indentation hardness systematically increases with residual contact radius a_p and decreases with the residual indentation profile diameter D_p. Lim and Chaudhri (1999) and Swadener et al. (2002a) tend to attribute the ISE to the different hardness values obtained for different spheres at the same value of the normalized contact radius $\omega = a_p/D_p$ (or equivalently at fixed effective plastic strain $p = c\,\omega$). Therefore, for the same contact radius, a smaller sphere penetrates to a greater depth than a larger sphere. This crucial experimental fact suggests that Hill et al. (1989) relation given by Eq. (36) characterizes the macroscopic hardness and does not incorporate the effect of strain gradients; thus, it cannot be used to interpret the ISE. Xue et al. (2002b) confirmed Tymiak et al. (2001) and Swadener et al. (2002b) experimental results by conducting a numerical study using the mechanism-based strain gradient (MSG) plasticity theory of Gao et al. (1999a) and Huang et al. (2000a). The numerical results showed the decrease and increase of indentation hardness with increasing residual contact radius a_p for a fixed geometry of pyramidal and spherical indenters (i.e. for a fixed spherical indenter's diameter D and a fixed conical indenter's angle θ), respectively.

Therefore, by substituting $a_p = \omega D_p$ into Eq. (33), one obtains a relation that can characterize the ISE for a constant ω, such that:

$$\left(\frac{H}{H_o}\right)^{\beta} = 1 + \left(\frac{D^*}{D_p}\right)^{\beta/2} \tag{37}$$

where D^* is a material specific parameter that characterizes the size dependence of the hardness and depends on the indenter geometry as well as on the plastic flow, such that it is given by:

$$D^* = \xi \ell \tag{38}$$

with

$$\xi = \frac{2}{c\bar{r}\omega} \tag{39}$$

and the macro-hardness H_o is given by

$$H_o = \kappa c^{1/m} \sigma_o \omega^{1/m} \tag{40}$$

It is worth mentioning that if $\beta = 2$ in Eq. (37), one retains the relation recently proposed by Swadener et al. (2002a), where they expand the Nix and Gao (1998) framework to include a wide variety of indenter shapes. Moreover, the characteristic form for the size dependence of the hardness presented by Eq. (37) gives a straight

line when the data are plotted as $(H/H_o)^{\beta}$ versus $D_p^{-\beta/2}$ for a given ω. The intercept of this line is 1 and the slope is $D^{*}\beta/2$. Moreover, Eq. (38) shows that D^{*} is a linear function of the length-scale parameter ℓ. Thus, D^{*} is a crucial parameter that characterizes the indentation size effect and its accurate experimental measure using spherical indenters yields a reasonable value for the material intrinsic length parameter as will be shown later in this section. H_o, D^{*}, and β are thus the material properties used to obtain the hardness predictions.

As we suggested earlier, Eq. (33) or Eq. (37) can be used to calibrate the length scale parameter ℓ from spherical indentation tests provided that the contact radius a_p and the indentation profile of diameter D_p are specified in the unloaded configuration. However, from an experimental point of view, the indentation depths in the loaded and unloaded configurations, h and h_p, are usually measured in the spherical indentation tests for a given indentation load P and spherical indenter diameter D, while the contact radius a_p is very difficult to measure. Thus, in order to be able to use Eq. (33) one needs first to calculate the residual contact radius a_p from the measurable parameters h and h_p. Moreover, one needs to specify the residual contact radius a_p in order to estimate the micro-hardness $H = P/\pi a_p^2$ and the macro-hardness H_o in Eq. (33) for a spherical indenter. As such, it is desirable to find a relationship between the indentation depths h and h_p and the contact radiusa_p. There are many geometric relationships available in the literature that are used to estimate a_p. A review of these relationships is given by Kucharski and Mroz (2001). This relationship, however, should be a function of the material properties since smaller yield strains and higher hardening exponents generally imply larger amounts of material flow, and hence, larger contact size (Begley and Hutchinson, 1998). For this purpose, we adopt the relations that were recently proposed by Kucharski and Mroz (2001) in order to calculate a_p and D_p in the unloaded configuration in terms of the measured parameters h and h_p, such that:

$$a_p = \sqrt{q^2 D_p h_p} \quad \text{and} \quad D_p = D\left(1 + \frac{0.38(h - h_p)}{h_p q^2}\right) \tag{41}$$

where D is the diameter of the spherical indenter and q^2 is a constant (mostly of the order of 1.0) dependent only on the exponent m and is defined by Tabor (1951) as follows:

$$q^2 = 2.5\left(\frac{2m-1}{4m+1}\right) \tag{42}$$

It has been argued by Swadener et al. (2002a) and Xue et al. (2002b) that the ISE for a spherical indenter is not related to the depth of indentation h_p. Xue et al. (2002b) also suggested that the macro-hardness (H_o) and the micro-hardness (H) increase with the contact radius a_p. However, this is only valid for a fixed indenter diameter D and not for a fixed ω, where the latter illustrates the ISE in spherical indentation as suggested above (i.e. different hardness values for different spheres). The substitution of D_p from Eq. (41) into Eq. (37) yields a relation that shows the depth dependence of micro-hardness on the indentation depth at a specific effective

plastic strain p (or equivalently at fixed ω), in contrast to the suggestion of Swadener et al. (2002a) and Xue et al. (2002b), such that:

$$\left(\frac{H}{H_o}\right)^{\beta} = 1 + \left(\frac{h^*}{h_p}\right)^{\beta/2} \tag{43}$$

where h^* is given as:

$$h^* = \zeta \ell \quad \text{with} \quad \zeta = \frac{2\omega}{c\bar{r}q^2} \tag{44}$$

Eq. (43) agrees with the finding of Stelmashenko et al. (1993), DeGuzman et al. (1993), Ma and Clarke (1995), Poole et al. (1996), McElhaney et al. (1998), Nix and Gao (1998) and many others followed (see the Introduction), who showed that the indentation hardness obtained using a conical or pyramidal indenters increases with decreasing indentation depth h_p. Moreover, this result agrees well with the experimental results of Tymiak et al. (2001) who showed for different spherical tip radii of few microns the decrease in indentation hardness with indentation depth for (100) aluminum.

To emphasize the above result, one can easily show that the GND density (ρ_G) nucleated and evolved underneath a spherical indenter [Eq. (28)] decreases with increasing the indentation depth h_p for a constant ω. By substituting D_p from Eq. (41) into Eq. (28) with $\omega = a_p/D_p$, one can rewrite ρ_G as a function of the indentation depth h_p as follows:

$$\rho_G = \frac{2\omega^2}{q^2 b_G h_p} \tag{45}$$

This qualitatively agrees well with the expression derived by Nix and Gao (1998) for the density of GNDs nucleated underneath a conical indenter $\left(\rho_G = 3\tan^2\theta/2b_G\bar{h}_p\right)$ where θ is the angle of indented surface that remains constant (for sharp constant angle indenters like a Berkovich or Vickers) similar to ω for the spherical indenter, such that $\tan\theta = \bar{h}_p/\bar{a}_p$ and $\omega = a_p/D_p$. Note that the superimposed bar designates data associated with a conical/pyramidal indenter.

Recently, a method was developed to determine the material length-scale using micro-hardness results from conical/pyramidal indenters (Abu Al-Rub and Voyiadjis, in press). A relation between the micro-hardness, $\bar{H}$, the macro-hardness, $\bar{H}_o$, and the length-scale parameter, $\bar{l}$, was given as follows (see Fig. 2):

$$\left(\frac{\bar{H}}{\bar{H}_o}\right)^{\beta} = 1 + \left(\frac{\bar{h}^*}{\bar{h}_p}\right)^{\beta/2} \tag{46}$$

where $\bar{H}_o$ and $\bar{h}^*$ are given as follows:

$$\bar{H}_o = \kappa\sigma_o \bar{c}^{1/m} (\tan\theta)^{1/m} \tag{47}$$

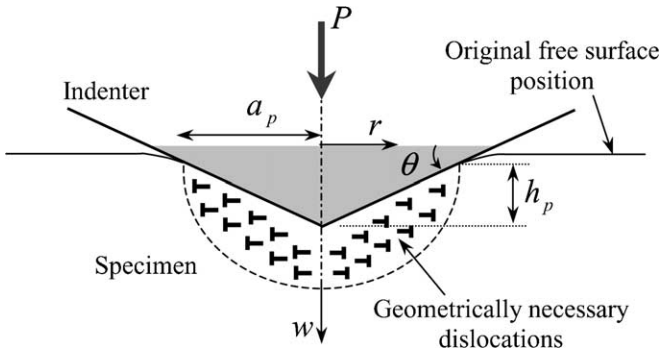

Fig. 2. Axisymmetric rigid conical indenter. Geometrically necessary dislocations created during the indentation process.

$$\bar{h}^* = \bar{\zeta}\,\bar{\ell} \quad \text{with} \quad \bar{\zeta} = \frac{3}{2\bar{c}\,\bar{r}}\tan\theta \tag{48}$$

The superimposed bar is used in the rest of this paper to distinguish the conical/pyramidal indenter parameters from those of the spherical indenter. The characteristic form for the depth dependence of the hardness presented by Eq. (46) gives a straight line when the data are plotted as $(\bar{H}/\bar{H}_o)^{\beta}$ versus $\bar{h}^{-\beta/2}$, with an intercept of 1 and a slope of $\bar{h}^{*\beta/2}$. The length-scale parameter $\bar{\ell} = \bar{h}^*/\bar{\zeta}$ can then be calculated using Eq. $(48)_1$, where $\bar{\zeta}$ is determined in terms of the shape of the conical indenter (i.e. $\tan\theta$) and the material properties (i.e. $\bar{r}$ and c) which are known. Therefore, by using Eq. (46) to fit the hardness experimental data obtained from indentation tests, one can simply compute the intrinsic length-scale parameter that characterizes the size effects using Eq. (48).

By setting $\beta = 2$ in Eq. (46), one retains the relation originally proposed by Nix and Gao (1998), where they found a linear dependence of the square of the micro-hardness, $\bar{H}^2$, to the inverse of the indentation depth, $1/\bar{h}_p$. Nix and Gao (1998), also, suggested that $\bar{h}^*$ and $\bar{H}_o$ are dependent and related through $\bar{h}^* = (81/2)b_S\alpha^2\tan^2\theta(G/\bar{H}_o)^2$. Their relation, thus, gives a similar argument to that of Eq. (48) which suggests that $\bar{h}^*$ is dependent on the shape of the indenter as well as on the material property. $\bar{c}$ is a material constant on the order of 1.0 which estimates the effective plastic strain under the conical/pyramidal indenter as $\bar{p} = \bar{c}(\bar{h}_p/\bar{a}_p) = \bar{c}\tan\theta$ (Johnson, 1970; Tymiak et al., 2001; Xue et al., 2002b). Note that for a constant angle pyramidal indenter θ, $\bar{h}_p/\bar{a}_p$ is constant, which implies that the plastic strain is independent of depth. However, h_p/a_p is not constant for spherical indenters as it is for perfectly sharp ones. Thus, unlike the spherical indenter, several conical or pyramidal indenters have to be used in order to determine the whole plastic behavior of the material. This emphasizes again the above suggestion that in order to characterize the ISE in hardness experiments by spherical indenters, the ratio of $\omega = a_p/D_p$ should be fixed or, equivalently, $p = c\omega$ should be constant; that

is, setting the plastic strain to be independent of the sphere size. By doing this, one draws an analogy of the ISE in spherical indentation similar to that in conical/pyramidal indentation.

Moreover, one can easily obtain a similar relation to Eq. (33) for conical or pyramidal indenters by substituting for $\bar{h}_p$ in Eq. (46) the relation $\bar{h}_p = \bar{a}_p \tan\theta$, such that:

$$\left(\frac{\bar{H}}{\bar{H}_o}\right)^{\beta} = 1 + \left(\frac{\bar{a}^*}{\bar{a}_p}\right)^{\beta/2} \tag{49}$$

where $\bar{a}^*$ is given as:

$$\bar{a}^* = \bar{\varsigma}\bar{\ell} \quad \text{with} \quad \bar{\varsigma} = \frac{3}{2\,\bar{c}\,\bar{r}} \tag{50}$$

The expression in Eq. (49) shows that the pyramidal indentation hardness $\bar{H}$ increases with decreasing the contact radius $\bar{a}_p$ (i.e. GNDs decreases with increasing contact radius, $\rho_G = 3\tan\theta/2b_G\bar{a}_p$). This result agrees well with the experimental observations for sharp indenters with constant indenter angle such as the Berkovich and Vickers indenters (e.g. Lim and Chaudhri, 1999; Tymiak et al., 2001; Gerberich et al., 2002; Swadener et al., 2002b, Elmustafa and Stone, 2002, 2003).

As a result of the above discussion, the analogy between the ISE observed in micro- and/or nano-hardness experiments by conical/pyramidal and spherical indenters is shown in Table 1. Note that the row before last in Table 1 shows that one can characterize the ISE by using $H = H_o\sqrt{1 + h^*/h_p}$ (i.e for $\beta = 2$) for either the micro-hardness or the nano-hardness, but not for both. This is called the bilinear ISE as noted for aluminum and alpha brass by Elmustafa and Stone (2002, 2003) for hardness results obtained using a pyramidal indenter. Elmustafa and Stone (2002, 2003) observed that when $(H/H_o)^2 = 1 + h^*/h_p$ is used to fit the experimental results, the data at deep indents (micro-hardness) exhibits a straight-line behavior, whereas for shallow indents (nano-hardness) the slope of the line severely changes, decreasing by a

Table 1
Indentation size effect (ISE) in conical/pyramidal and spherical indenters

Property	Conical/pyramidal indenter[a]	Spherical indenter
ISE [Hardness $\uparrow \leftrightarrow$ depth $\downarrow$]	Fixed θ or p	Fixed ω or p
Effective plastic strain, p	$p = c(h_p/a_p) = c\tan\theta$	$p = c(a_p/D_p) = c\,\omega$
Effective plastic strain gradient, η	$\eta = 3\tan^2\theta/2\bar{r}h_p$	$\eta = 2\omega^2/q^2\bar{r}h_p$
Length-scale parameter, $\ell = h^*/\zeta$	$\zeta = 3\tan\theta/2c\bar{r}$	$\zeta = 2\omega/q^2c\bar{r}$
Macro-hardness, H_o	$H_o = \kappa\sigma_o c^{1/m}(\tan\theta)^{1/m}$	$H_o = \kappa\sigma_o c^{1/m}(\omega)^{1/m}$
Micro- or nano-hardness, H (bilinear ISE)	$H = H_o\sqrt{1 + h^*/h_p}$	$H = H_o\sqrt{1 + h^*/h_p}$
Micro- and nano-hardness, H	$H = H_o\sqrt[\beta]{1 + (h^*/h_p)^{\beta/2}}$	$H = H_o\sqrt[\beta]{1 + (h^*/h_p)^{\beta/2}}$

[a] Note that the superimposed bar, which is used to distinguish conical parameter from spherical, has been removed.

factor of 10, resulting in a bilinear behavior. However, the relation in the last row of Table 1 has been used successfully by Abu Al-Rub and Voyiadjis (in press) to fit both micro- and nano-hardness values (i.e. for deep and shallow indents, respectively) obtained using pyramidal indenters. Different positive values of β for different materials have been used to fit the data. We believe that β is a material property that contributes as an "interaction coefficient" which assesses the proper coupling between the SSD density (ρ_S) and the GND density (ρ_G) [see Eq. (9)] during indentation or, equivalently, the coupling between the effective plastic strain (p) and its gradient (η) [see Eq. (2)]. This coupling cannot be simply linear (i.e. obstacles of a similar strength) as advocated by many authors (e.g. Kocks et al., 1975; Ma and Clarke, 1995; Poole et al., 1996; Nix and Gao, 1998). Similar argument has been made by Fleck and Hutchinson (1997), Begley and Hutchinson (1998), Stolken and Evans (1998), and Zaiser and Aifantis (2003). However, no attempt has been made until now to study the effect of β on solving the size effect problems with the aid of the gradient theory.

It should also be stated here that the above interpretation of the ISE is based on the evolution of the GNDs, while from time to time in the literature; several important factors in experiments (e.g. interfacial friction, indenter pile-up or sink-in, loading rate, oxidation layer, etc.) have been though to be responsible for the ISE. Excellent review of these factors is given by Xue et al. (2002b). However, careful experimental studies have excluded these factors from being completely responsible for the ISE (Xue et al., 2002b).

3.2. Identification of the length-scale

The above identification theory is first applied to the micro- and nano-indentation results obtained by Swadener et al. (2002a) for spherical indentation of annealed iridium. The contact radii a_p were measured by atomic force microscopy (AFM). The spherical indentation was conducted using 14, 69, 122, 318, and 1600 μm spheres for which plots of the mean values of hardness versus the normalized contact radius $\left(\omega = a_p/D_p\right)$ were presented. The plots showed a monotonic increase in hardness with increasing ω. However, the experimental results showed a decrease in hardness with increasing D_p at the same value of ω and thus at the same value of the effective plastic strain (since $p = c\,\omega$). This illustrates the ISE as proposed by Eq. (37) for spherical indenters.

It is worth to mention that all the experiments used here in identifying the length-scale parameter were conducted at room temperature. Furthermore, it was also reported that no damage occurred in the material beneath the indenter such that the measured micro- and nano-hardness data provides a true measure of the plastic properties of the material. Micro- and nano-hardness thus provide a convenient tool for the identification of the plasticity intrinsic material length-scale, provided damage is avoided.

Following the procedure proposed above for identification of the material length parameter, the hardness results obtained from micro- and nano-indentation tests can be displayed as a plot of $(H/H_o)^\beta$ versus $D_p^{-\beta/2}$ such that the slope of the

resulting straight line is $D^{*\beta/2}$ [see Eq. (37)]. Fig. 3 shows the ISE for $\omega = 0.025$ (1% effective plastic strain) for the five spherical tips. In this figure a comparison of the present model with the Swadener et al. (2002a,b) model is also shown. It is obvious that the present model with $H_o = 0.9$ GPa, $\beta = 0.85$, $D^* = 52$ μm (different than $\beta = 2$ and $D^* = 500$ μm of Swadener et al., 2002a,b, model) agrees well with the experimental results for small and large spheres; while the Swadener et al.'s model overestimates the hardness at small values of D_p and it fits the data well for $D_p > 100$ μm. The dimensionless parameter $\xi = 100$ given by Eq. (39) for $c = 0.4$, $\omega = 0.025$, and $\bar{r} = 2$ can now be used to estimate the material length parameter to be $\ell = 0.52$ μm using Eq. (38) with $D^* = 52$ μm.

The above identification procedure is also applied to the nano-indentation hardness results of Lim et al. (1998 and Lim and Chaudhri, 1999) for spherical indentation of polycrystalline annealed and work-hardened oxygen free copper (OFC). The projected contact areas of the nano-indentations were measured using AFM and were used for determining the nano-hardness values. The variation in the hardness with a_p/D was determined using spherical indenters of diameters 14, 60, 120, 400, and 1000 μm. The value of D_p was not reported there, but is assumed here to be $1.1D$. Fig. 4 shows the ISE for $\omega = 0.025$ (1% effective plastic strain) for different spheres. The comparison of the present model [Eq. (37)] and the Swadener et al.'s model with the experimental results shows, once again, that our proposed model with β having different values than 2 fits the results very well, while the Swadener et al.'s model overestimates the hardness values at small indentation diameters of $D_p < 40$ μm. A plot of $(H/H_o)^\beta$ versus $D_p^{-\beta/2}$ using the present model is also shown in Fig. 4. Two different sets of data have been used to fit the experimental results for OFC: $H_o = 0.12$ GPa, $\beta = 0.88$, $D^* = 79$ μm for annealed OFC and $H_o = 0.87$ GPa, $\beta = 0.8$, $D^* = 0.114$ μm for work-hardened OFC. Note that H_o corresponds to the saturation value when the hardness H does not change as the indentation size increases. Using $\xi = 100$, as determined above for annealed iridium, implies that $\ell = 0.79$ μm and $\ell = 1.14$ nm for annealed and work-hardened OFC, respectively. A summary of the fitting results is included in Table 2.

As suggested by Eq. (20), the material length parameter is proportional to the mean spacing between the SSDs (L_S) or equivalently to the density of the SSDs (ρ_S). One may, therefore, question the difference between the estimated values of ℓ for both annealed and work-hardened OFC although they are obtained at the same plastic strain value of 1%. However, one can note that ℓ for the work-hardened OFC is smaller than that for the annealed OFC. This indicates that the spacing between the SSDs is reduced in the heavily work-hardened specimen due to the higher presence of prior dislocation density caused by the method of specimen preparation. Lim and Chaudhri (1999) reported that they cold-worked the OFC to a large strain value of approximately 60%. This means that the work-hardened specimen initially contains higher dislocation density, or equivalently smaller mean spacing between dislocations, and thus smaller material length parameter. The presence of prior dislocations, thus, affects the estimation of the material length parameter to yield higher hardness values. The shear stresses required to move dislocations in the work-hardened OFC will be higher than that required for the

annealed OFC (owing to the interactions of nucleated dislocations with prior dislocations caused by work-hardening); thus, the nano-hardness of the latter is smaller than that of the former which is confirmed by the experimental results in Fig. 4(a) and (b). Moreover, from compression tests of annealed and work-hardened OFC (Lim and Chaudhri, 1999), it is noticed that the work hardening results in an increase in the flow stress of 0.29 GPa for work-hardened OFC compared to the flow stress of the annealed OFC at 1% plastic strain. This indicates that materials with smaller ℓ are harder, and require greater loads to create the same contact area. This is consistent with both the experimental behavior and anticipated behavior of the constitutive description, which dictates that the additional amount of hardening during deformation increases as ℓ increases.

Furthermore, the material length of work-hardened OFC is close to the conventional plasticity limit (i.e. $\ell = 0$), indicating that the size effect in work-hardened OFC is not significant as compared to that in annealed OFC. This is supported by the ISE results presented in Fig. 4. At $D_p > 1000$ μm the measured hardness for the annealed OFC is still decreasing with increasing D_p and has not yet reached a plateau value corresponding to a macroscopic hardness (H_o), whereas at $D_p > 400$ μm the measured hardness for cold-worked OFC reaches a value with no further decrease in hardness and corresponds to a macroscopic hardness of $H_o = 0.87$ GPa. Thus, for OFC with this degree of cold-work, very little additional work hardening occurs during indentation. This observation is also supported by the hardness results for the annealed iridium presented in Fig. 3, where the value of H_o is somewhat overestimated. Even at $D_p > 3500$ μm, the measured hardness is

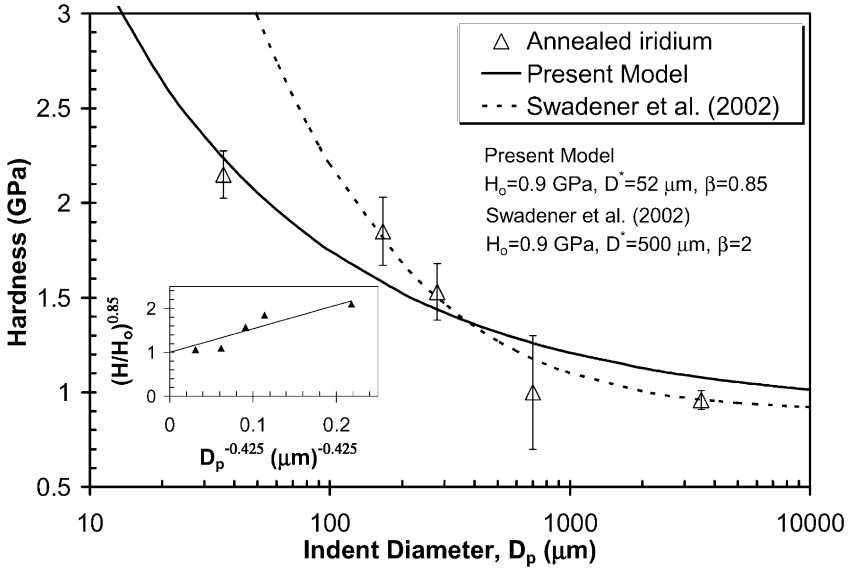

Fig. 3. Indentation size effect in annealed iridium measured with spherical indenters (Swadener et al., 2002a): comparison of experiments at $\omega = 0.025$ ($p = 1\%$) with the proposed model and Swadener et al.'s model.

still decreasing with increasing D_p and has not yet reached a plateau value corresponding to H_o. One can thus conclude that the size effect is more significant in annealed specimens than in cold-worked specimens. Therefore, the indentation size effect is expected to be influenced by prior dislocations and the additional work

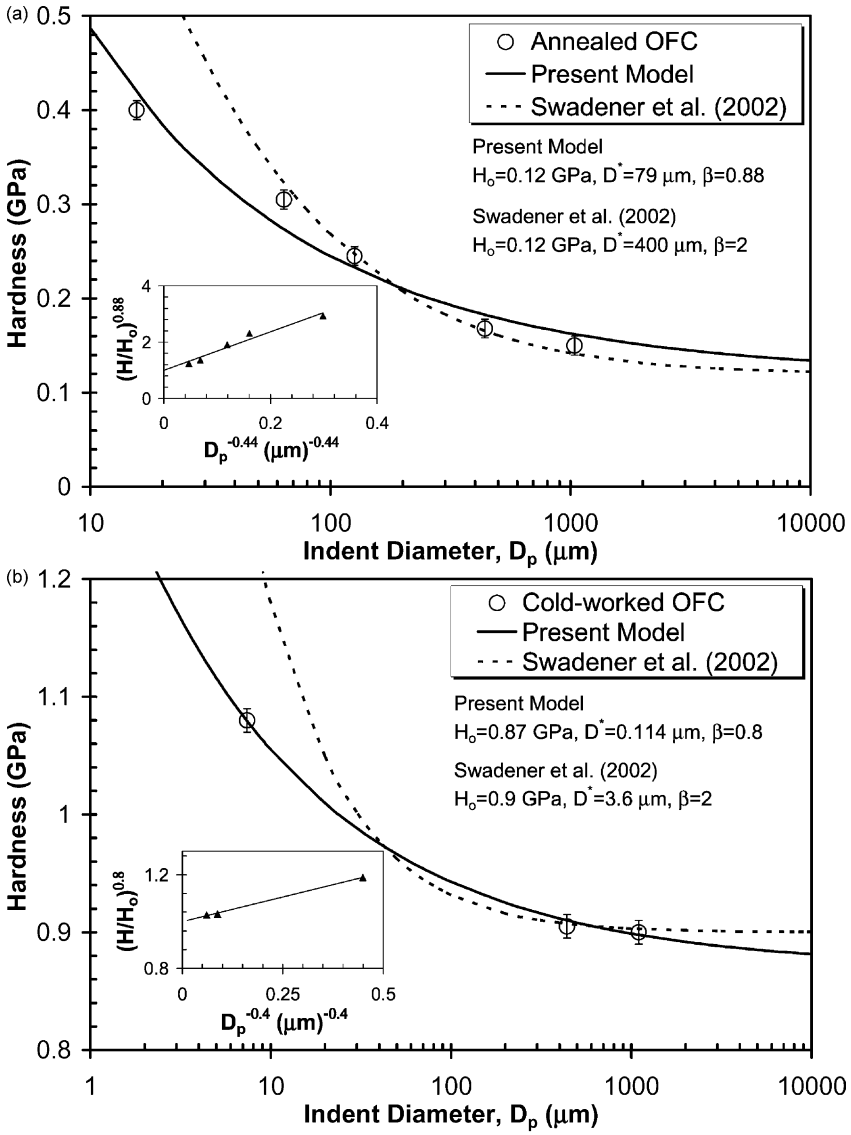

Fig. 4. Indentation size effect in oxygen-free copper (OFC) measured with spherical indenters (Lim et al., 1998; Lim and Chaudhri, 1999): comparison of experiments at $\omega = 0.025$ ($p = 1\%$) with the proposed model and Swadener et al. (2002a,b) model: (a) annealed OFC; (b) work-hardened OFC.

Table 2
Values of the material length-scale parameter ℓ from the fitted micro- and nano-indentation experiments

Material	β	Spherical indenter at $p = 0.01$				Pyramidal indenter[a] at $p = 0.07$			
		H_o (GPa)	D^* (μm)	ζ	$\ell = D^*/\zeta$ (μm)	H_o (GPa)	h^* (μm)	ς	$\ell = h^*/\varsigma$ (μm)
Annealed irridium (Swadener et al. 2002a,b)	0.85	0.90	52.0	100	0.52	2.5	0.226	1.3	0.17
Annealed OFC (Lim et al. 1998; Lim and Chaudhri, 1999)	0.88	0.12	79.0	100	0.79	0.44	0.486	1.3	0.37
Work-hardened OFC (Lim et al. 1998; Lim and Chaudhri, 1999)	0.80	0.87	0.114	100	0.001	0.87	0.017	1.3	0.013

[a] Note that the superimposed bar, which is used to distinguish conical/pyramidal parameter from spherical, has been removed.

hardening that occurs during indentation, which is compensated for by using the interaction coefficient β. This is further elaborated in Section 5.

As shown in Figs. 3 and 4, predictions from the Swadener et al. (2002a,b) model overestimates hardness for small values of D_p. This discrepancy can be largely corrected by changing the value of the interaction coefficient β, which is equal to 2 in Swadener et al. model. The interaction coefficient β compensates for the proper coupling between the SSDs and GNDs during indentation. This coefficient may resolve a number of discrepancies if addressed properly. Therefore, the most likely source of impediment in the Swadener et al.'s model is due to the assumption that the SSD and GND densities are coupled in a linear sense (i.e. obstacles are of a similar strength).

In addition, Nix and Gao (1998) interpreted the ISE as an increase in the hardness values with decreasing in the depth of indentation, while Swadener et al. (2002a) showed a dependence of hardness on the diameter of the indenter rather than on the depth of indentation. This controversy in interpreting the ISE is explained earlier in this work (see Table 1). It is shown that the ISE in spherical indenters can still be interpreted as an increase in hardness with decreasing indentation depth, or equivalently with increasing contact radius, which is given by Eqs. (43) and (33). This is clearly demonstrated in Fig. 5 for the three sets of indentation data (obtained at $\omega = 0.025$) associated with annealed iridium, and annealed and work-hardened OFC. The experimental data in Fig. 5(a) and (b) are fitted very well by our model given by Eqs. (43) and (33) with $c = 0.4$, $\bar{r} = 2$, $q = 1$, and the corresponding ℓ values are given in Table 2. With confidence, one may thus conclude that the ISE is interpreted as a decrease in the hardness with increase in the indent size for various indenter geometries.

Lim and Chaudhri (1999) and Swadener et al. (2002a,b) have conducted an experimental investigation of indentation size effect using pyramidal indenters on OFC and iridium, respectively. One can estimate the material length parameter $\bar{\ell}$

from those hardness results by following the procedure that is briefly outlined above [see Eqs. (46)–(48) and Table 1] and thoroughly described in Abu Al-Rub and Voyaidjis (in press) for identification of $\bar{\ell}$ obtained from conical/pyramidal indentation tests. The hardness results obtained from nano- and micro-indentations using,

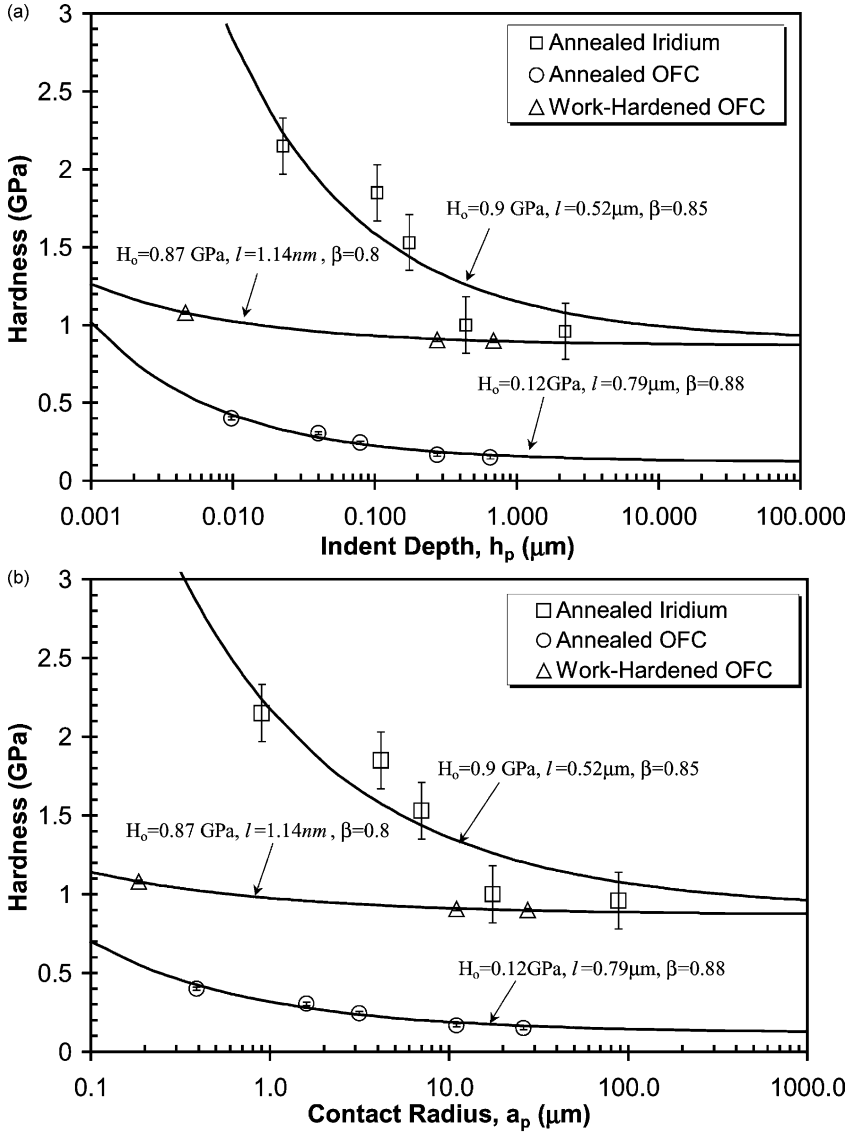

Fig. 5. Indentation size effect in iridium and oxygen-free copper measured with spherical indenters (Lim et al., 1998; Lim and Chaudhri, 1999; Swadener et al., 2002a): comparison of experiments at $\omega = 0.025$ ($p = 1\%$) with the proposed model: (a) hardness versus indentation depth [Eq. (43)]; (b) hardness versus contact radius [Eq. (33)].

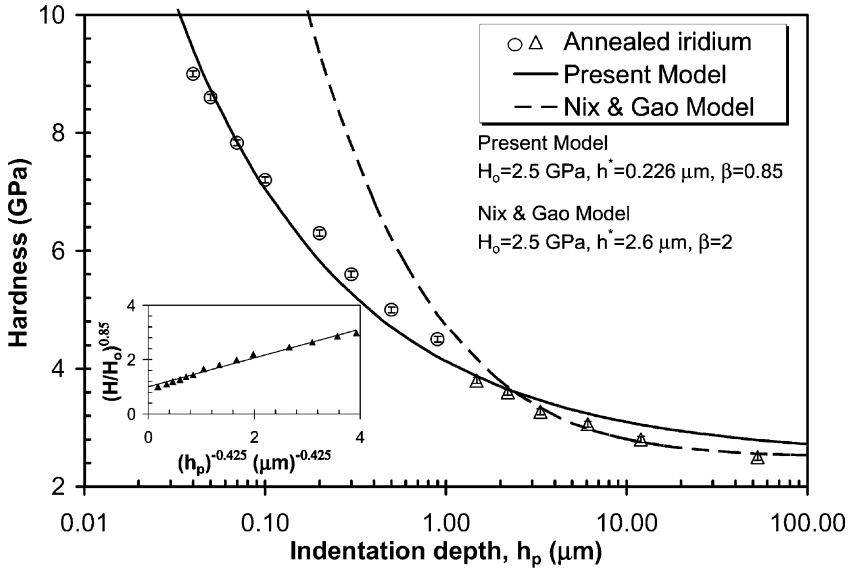

Fig. 6. Indentation size effect in annealed iridium measured with a Berkovich indenter (Swadener et al., 2002a) and comparison of experiments with the proposed model and Nix and Gao (1998) model. Δ and ○ designate microhardness and nanohardness data, respectively.

respectively, Berkovich and Vickers indenters are plotted in Figs. 6 and 7. Also in these figures, plots of the present model as $\left(\bar{H}/\bar{H}_o\right)^{\beta}$ versus $\bar{h}_p^{-\beta/2}$ and the Nix and Gao (1998) model predictions are shown. The values of $\bar{H}_o$, $\bar{h}^*$, β used to fit the experimental results are shown in these figures. The prediction of our model agrees well with the micro- and nano-hardness data, while the Nix and Gao (1998) model prediction diverges significantly from the nano-hardness results for $\bar{h}_p < 1$ μm. This confirms that the inclusion of the interaction coefficient β largely corrects the discrepancy in Nix and Gao's model prediction. If an intrinsic lattice stress is included, as suggested by Qui et al. (2001), or an additional hardness term is added, as suggested by Swadener et al. (2002b), they provide only a marginal improvement of predictions of the Nix and Gao (1998) model.

The dimensionless parameter $\bar{\zeta} = 1.343$ is calculated using Eq. $(48)_2$ assuming that $\bar{c} = 0.2$ (corresponds to 7% effective plastic strain as reported by Johnson, 1970), the Nye factor $\bar{r} = 2$ (Arsenlis and Parks, 1999), and $\tan\theta = 0.358$ (McClintock and Argon, 1966). The calculation of $\bar{\ell}$, therefore, depends strongly on the material parameters $\bar{c}$ and $\bar{r}$. The resulting values for the material intrinsic length-scale, outlined in Table 2, are in the range of sub micrometers. This confirms well with the observations of Begley and Hutchinson (1998), Nix and Gao (1998), Stolkend and Evans (1998), and Yuan and Chen (2002). Moreover, one can note that $\bar{\ell}$ for the cold-worked sample is smaller than the value for the annealed sample, indicating that spacing between statistically stored dislocations is reduced in the hardened-worked material. However, it can be seen from Fig. 7(a) and (b) that for low

indentation depths of 150–200 nm, the nano-hardness values of both the work-hardened and the annealed OFC are almost the same (Lim and Chaudhri, 1999). This may indicate that at small indentation depths, the size of the nucleated dislocation cells (i.e. patterns), which can be assumed proportional to the mean free path of dislocations (L_S), are the same for both work-hardened and annealed OFC. Hence,

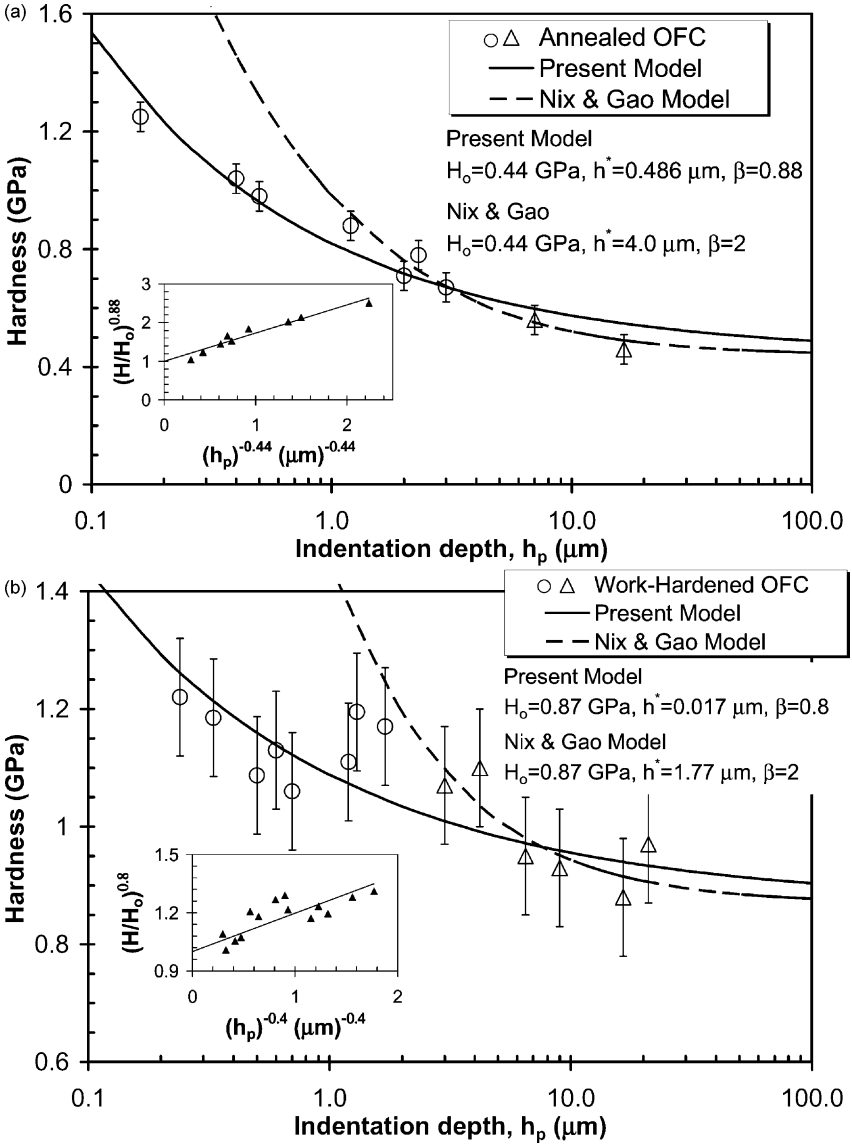

Fig. 7. Indentation size effect in oxygen free copper (OFC) measured with (Δ) Vickers and (○) Berkovich indenters (Lim et al., 1998; Lim and Chaudhri, 1999) and comparison of experiments with the proposed model and Nix and Gao (1998) model: (a) anealed OFC; (b) work-hardened OFC.

the length scale measures, which control the indentation size effect in both work-hardened and annealed OFC, at these small indents are expected to be the same. Thus, the shear stresses required for nucleation and expansion of these dislocation cells, or equivalently the nano-hardness values [Eq. $(22)_1$], are the same. Also, at those indents the prior dislocation densities have little effect on the nano-hardness values or the material length parameter. However, for $\bar{h}_p > 200$ nm it can be seen from Fig. 7 that the nano-hardness for both work-hardened and annealed OFC decreases gradually but, for all indentation depths, the nano-hardness of the worked-hardened OFC is larger than that of the annealed OFC. Accordingly, the length scale measures for both work-hardened and annealed OFC at $\bar{h}_p > 200$ nm are different. However, $\bar{\ell}$ for the latter is bigger than that of the former indicating that the interaction of the nucleated dislocation patterns with prior dislocations becomes significant. This suggests that the length scale parameter depends on the plastic strain level as suggested by Aifantis (1999) and Abu Al-Rub and Voyiadjis (in press), as well as on the prior dislocation density. This will be discussed thoroughly in Section 5.

It can be seen from the results presented in Figs. 3–7 that as the indentation size becomes much larger than the material-length scale parameter, the gradient effects become smaller and the corresponding hardness does not exhibit any indentation size effect. Moreover, the linearity of the data when plotted as $(H/H_o)^{\beta}$ versus $h_p^{-\beta/2}$ with different values of β implies that a linear addition law of ρ_S and ρ_G is

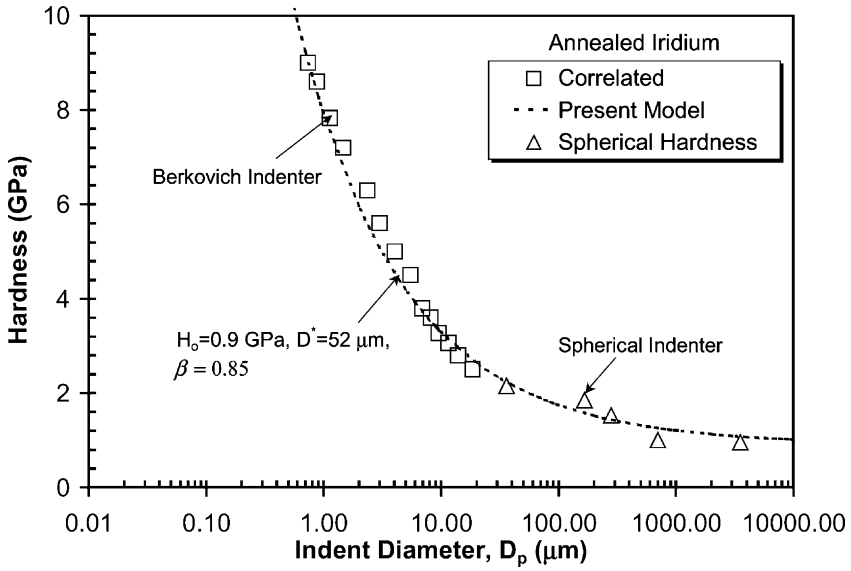

Fig. 8. Correlation of the indentation size effect in annealed irridium measured with a spherical indenter at $\omega = 0.025$ (Δ), correlated from a Berkovich indenter Eq. (55) (□) (data from Swadener et al., 2002a), and comparison of experiments with the proposed model Eq. (37) (dotted line).

inappropriate at the micro- and nano-scales. Recently, Zaiser and Aifantis (2003) adapted this simple linear addition law to derive a gradient plasticity law based on dislocation dynamics and concluded that GND density does not simply add up to the SSD density, which confirms our finding.

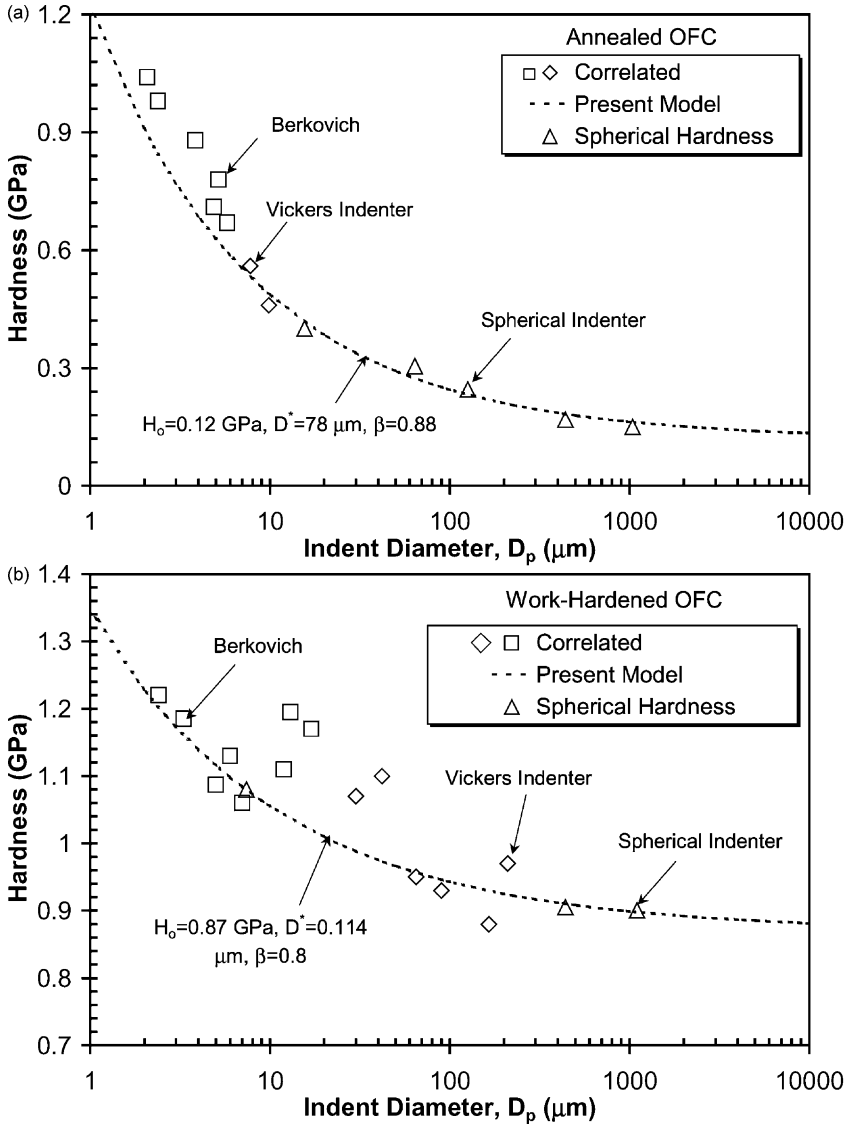

Fig. 9. Correlation of the indentation size effect in oxygen-free copper (OFC) measured with a spherical indenter at $\omega = 0.025$ (Δ), correlated from Vickers (◇) and Berkovich (□) indenters Eq. (55) (data from Lim et al., 1998; Lim and Chaudhri, 1999), and comparison of experiments with the present model Eq. (37) (dotted line): (a) annealed OFC; (b) cold-worked OFC.

4. On the correlation of hardness from spherical and pyramidal experiments

Hardening affects both the conical/pyramidal hardness and the spherical hardness, but in a different manner. Johnson (1970) has shown that the hardness measured by a Berkovich or a Vickers indenter corresponds to an effective plastic strain of 7% (i.e. at $\bar{p} = 0.07$), while the hardness values measured by spherical indenters are determined at an effective plastic strain of 1% (i.e. at $p = 0.01$). However, a correlation of the indentation size effect measured with the two indenter geometries (spherical and conical/pyramidal) can be determined by equating the hardness values evaluated from each indenter. The purpose of this section is therefore to bring hardness values measured by a conical indenter into the range of a spherical hardness data. Therefore, we seek a relation between the diameter of a spherical indenter, D_p, and the indentation depth of a conical/pyramidal indenter, h_p. By requiring that the hardness measured by the spherical indenter [i.e. H given by Eq. (37)] and that of a conical/pyramidal indenter (i.e. $\bar{H}$ given by Eq. (46)] be the same, one can easily show that D_p and h_p are related as follows:

$$D_p = \chi^2 D^* \left[\left(1 - \chi^\beta\right) + \bar{h}^* \beta/2 \, \bar{h}_p^{-\beta/2} \right]^{-2/\beta} \tag{51}$$

where $\chi = H_o/\bar{H}_o$ is a macroscopic parameter expressed as the ratio of the spherical macroscopic hardness to that of the conical/pyramidal indenter. Note that the interaction coefficient β is assumed to be the same for the two indenter geometries when the hardness value is the same (this assumption is concluded by fitting our model with the experimental results in Figs. 3 and 6 and Figs. 4 and 7). Yet, Eq. (51) is not satisfactory in obtaining D_p from the measured h_p since a relation between D^* and $\bar{h}^*$ is required.

The macroscopic parameter χ can be obtained from Eqs. (40) and (47) along with the effective plastic strain which is given by $p = c\omega$ for the case of pyramidal indenters and $\bar{p} = \bar{c}\tan\theta$ for the case of spherical indenters, such that:

$$\chi = (p/\bar{p})^{1/m} \tag{52}$$

p and $\bar{p}$ can also be expressed in terms of the SSD density, ρ_S, by using Eq. (17). Furthermore, by assuming that the mean free path between SSDs (L_S) is inversely proportional to the square root of the density of SSDs (i.e. $L_S \propto 1/\sqrt{\rho_S}$) and making use of Eq. (20) in order to express L_S in terms of ℓ or $\bar{\ell}$, one can write a relation between the material lengths of conical/pyramidal and spherical indenters, ℓ and $\bar{\ell}$, respectively, as follows:

$$\ell = \chi^{-m} \bar{\ell} \tag{53}$$

Making use of Eqs. (38) and (39) for expressing ℓ in terms of D^* (i.e. $\ell = D^*/\xi$) and Eqs. $(48)_1$ and $(48)_2$ for expressing $\bar{\ell}$ in terms of $\bar{h}^*$ (i.e. $\bar{\ell} = \bar{h}^*/\bar{\xi}$) along with Eqs. (52) and (53), one obtains a relation between D^* and $\bar{h}^*$ as follows:

$$D^* = \frac{4}{3}\left(\frac{\bar{c}}{c\omega}\right)^2 \bar{h}^* \tag{54}$$

By substituting D^* given by the above equation into Eq. (51), one obtains a relation that can be used to estimate D_p for a spherical indent from a measured h_p value of a conical/pyramidal indent, such that:

$$D_p = \frac{4}{3}\left(\frac{\bar{c}\chi}{c\omega}\right)^2 \left[(1-\chi^\beta)\bar{h}^{*-\beta/2} + \bar{h}_p^{-\beta/2}\right]^{-2/\beta} \tag{55}$$

Hence, the above equation can be used to bring the hardness values measured with a pyramidal indenter into the range of the spherical data by knowing $\bar{h}^*$ and β that are calibrated from the pyramidal hardness experimental data with the aid of Eqs. (46)–(48). Fig. 8 shows this correlation for annealed iridium by using Eq. (55) and plotting the hardness measured by spherical indenters (Swadener et al., 2002a) at $\omega = 0.025$. From Table 2, the values $c = 0.4$, $\bar{c} = 0.2$, $\beta = 0.85$, $\chi = 0.36$, and $\bar{h}^* = 0.226$ μm are used to find the D_p value that corresponds to $\bar{h}_p$ measured by the Berkovich indenter. Moreover, the proposed correlation agrees very well with the predictions of our model, Eq. (37), given $D^* = 52$ μm and $\beta = 0.85$ as listed in Table 2, which corroborates the proposed correlation.

The above correlation, Eq. (55), is also applied to the results obtained by Lim et al. (1998; Lim and Chaudhrie, 1999) for spherical and pyramidal indentation of OFC, which were presented in Figs. 4 and 7 for $\omega = 0.025$. The values of the parameters to be used in Eq. (55) are as outlined in Table 2 for both annealed and work-hardened OFC. It can be seen from Fig. 9 that the proposed correlation brings the spherical and pyramidal indenter results into agreement. In addition, using the values of H_o, D^*, and β for OFC from Table 2, we show in Fig. 9 that the hardness predicted by Eq. (37) agrees well with the correlated results. Note that the proposed model with the interaction coefficient β agrees well with micro-hardness results, as well as with the nano-hardness results.

5. Discussion

It was noted from previous results, which are summarized in Table 2, that the hardest materials have the smallest values of ℓ; the material intrinsic length of the work-hardened (hard) OFC is much smaller than that of the annealed (soft) OFC. A similar observation has been emphasized by Begley and Hutchinson (1998), Nix and Gao (1998), Stolkend and Evans (1998), Yuan and Chen (2002), and recently by Abu Al-Rub and Voyiadjis (in press). In addition, the calibrated values of ℓ from spherical indentation are different than those from pyramidal indentation. ℓ was determined at a specific plastic strain level of 0.01 in the case of spherical indentation and 0.07 in the case of pyramidal indentation. However, it was found that ℓ from spherical indentation are smaller than those from pyramidal indentation (see

Table 2), except for those of work-hardened OFC that exhibits less ISE. This suggests that ℓ generally decreases as the plastic strain level increases as was also assumed by Aifantis (1999) and Abu Al-Rub and Voyiadjis (in press). This reflects the decrease of the gradient influence with the increase of the effective plastic strain; corresponding to the gradual failure of microstructural plastic deformation carriers. Furthermore, this is consistent with the fact that the free slip distance L_S of dislocations decreases with hardness increase and that ℓ is related to L_S, which confirms the finding in Eq. (20) that reveals that ℓ is proportional to L_S. In fact, Gracio (1994) speculated that in copper, L_S decreases when the plastic strain increases and being equal to the grain size at the beginning of the deformation, and saturating towards values on the order of micrometer after a strain of only about 0.1. Moreover, Begley and Hutchinson (1998) showed that ℓ has different values for different hardening exponents m. Stolken and Evans (1998) also showed that ℓ does not change if m is constant. Aifantis and his co-workers (1999) proposed a phenomenological relation for the gradient coefficient as a function of the plastic strain and m. The suggestions of these authors are confirmed by the results in the previous sections, where the results showed a dependence of ℓ on the plastic strain level, as well as on the hardening level. The hardening exponents are $m = 8.9$, $m = 2$, and $m \to \infty$ for the annealed iridium, annealed and work-hardened OFC, respectively. It can be seen from Table 2 that ℓ is the highest for the annealed OFC, followed by that of annealed iridium, and finally that of work-hardened OFC. Thus, one concludes that as m decreases ℓ increases; that is, the material intrinsic length-scale increases as the amount of additional work-hardening after deformation increases.

Gracio (1994) approximated the evolution of mean dislocation spacing L_S with the following equation:

$$L_S = \frac{\delta d}{\delta + d p^{1/m}} \tag{56}$$

where d is the grain size, and δ is a constant coefficient on the order of 1.0 μm. Thus, from Eq. $(20)_1$, one can write ℓ in terms of the grain size d and the effective plastic strain p as follows:

$$\ell = \frac{\hbar \delta d}{\delta + d p^{1/m}} \tag{57}$$

It is worth noting that the above expression includes the case of a constant ℓ when $p = 0$, such that ℓ is proportional to the grain size d (i.e. $\ell = \hbar d$ when $p = 0$). In order to confirm the above conclusions, the ISE can be plotted for different plastic strain levels (i.e. different values of $\omega = a_p/D_p$ if using the spherical indenter or of $\tan\theta = h_p/a_p$ if using the pyramidal indenter). Fig. 10(a) shows the ISE for annealed iridium by spherical indenters (Swadener et al., 2002a) for ω =0.025, 0.05, 0.075, 0.1 (or for effective plastic strains of 0.01, 0.02, 0.03, 0.04, respectively), which are fitted by Eq. (37). With the aid of Eqs. (38) and (39), one can estimate ℓ for each ω, such that the variation of ℓ with the effective plastic strain is shown in Fig. 10(b). Similarly, Fig. 11(a) shows the ISE for annealed OFC by spherical indenters (Lim et al., 1998; Lim and Chaudhri, 1999) for $\omega = 0.025$, 0.05, 0.01, 0.15 (or for effective plastic

strains of 0.01, 0.02, 0.04, 0.06, respectively). The intrinsic material length-scale can then be assumed to decrease from an initial value ℓ_o at yield to a final value of $\ell \to 0$ at saturation (corresponds to the conventional plasticity limit) at a rate characterized by a constant coefficient k_1, such that:

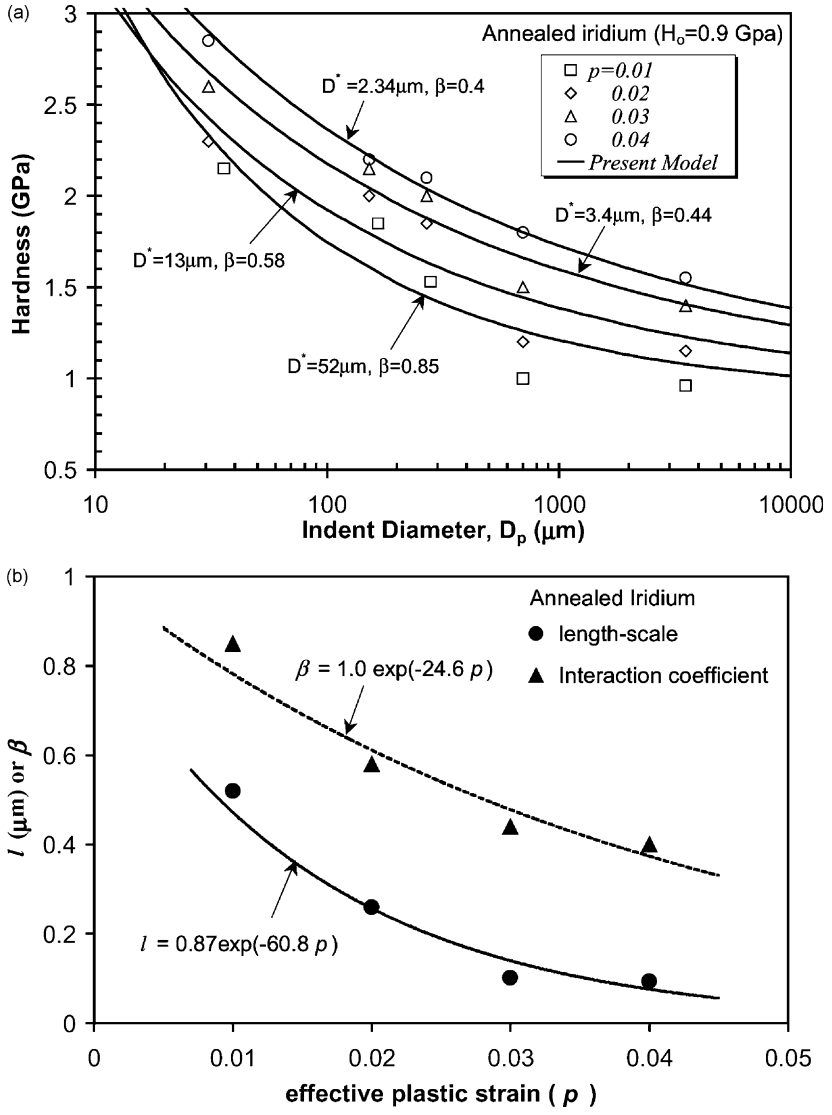

Fig. 10. The indentation size effect in annealed iridium: (a) measured with a spherical indenter at $\omega = 0.025$ (□), $\omega = 0.05$ (◇), $\omega = 0.075$ (Δ), $\omega = 0.1$ (○) (data from Swadener et al., 2002a,b), and comparison of experiments with the present model Eq. (37) (solid lines); (b) variation of intrinsic material length-scale (ℓ) and the interaction coefficient (β) with the effective plastic strain (p), and comparisons with the corresponding Eqs. (58) and (59), respectively.

$$\ell = \ell_o \exp(-k_1 p) \tag{58}$$

This two-parameter function is thought to give enough freedom for the evolution of the material intrinsic length-scale, and is consistent with the experimental trends presented in Figs. 10(b) and 11(b). The coefficient k_1 is characterized by the hardening

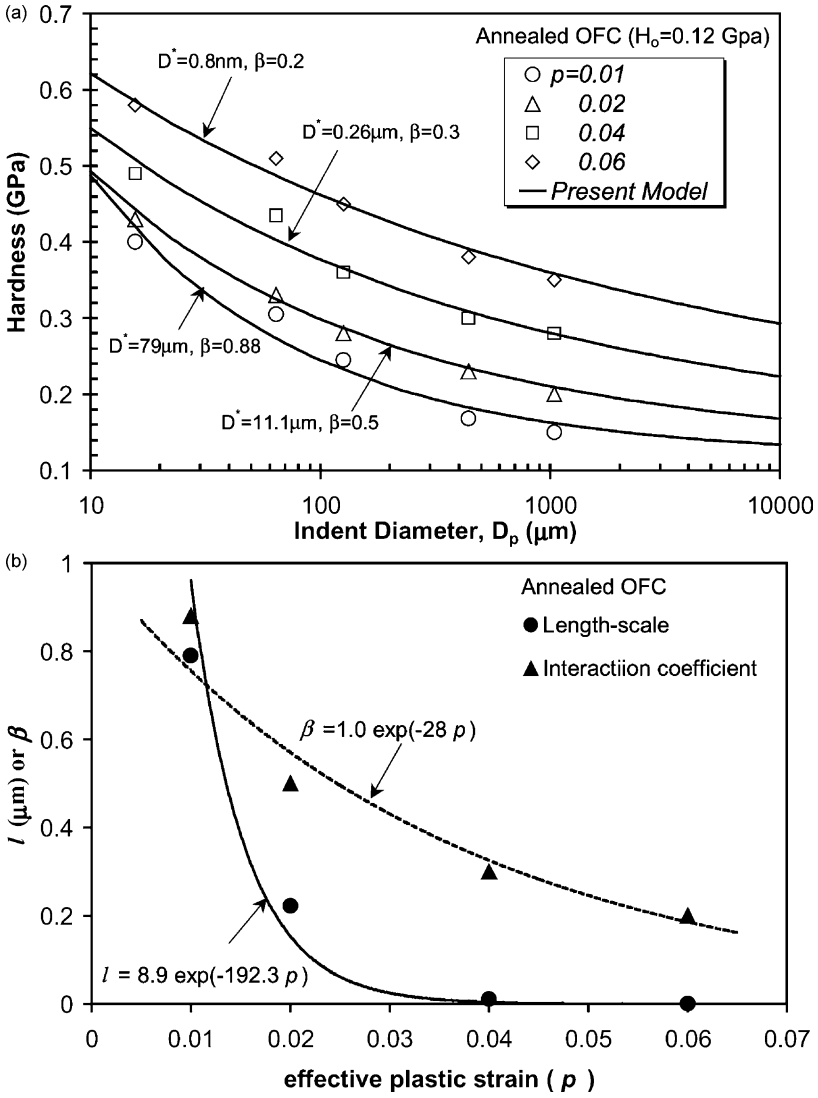

Fig. 11. The indentation size effect in annealed oxygen-free copper: (a) measured with a spherical indenter at $\omega = 0.025$ (○), $\omega = 0.05$ (Δ), $\omega = 0.1$ (□), $\omega = 0.15$ (◇) (data from Lim et al., 1998; Lim and Chaudhri, 1999), and comparison of experiments with the proposed model Eq. (37) (solid lines); (b) variation of intrinsic material length-scale (ℓ) and the interaction coefficient (β) with the effective plastic strain (p), and comparisons with the corresponding Eqs. (58) and (59), respectively.

exponent m. In addition, the case of a constant length-scale $\ell = \ell_o$ at yield ($p = 0$) indicates that size effect is present even in the elastic domain, where $\ell = \ell_o$ corresponds to the effect of prior dislocation density, which can be a combination of ρ_S and ρ_G, that is nucleated during the specimen preparation. For instance, in tensile tests the decrease in the initial yield stress with size (Stolken and Evans, 1998) could be explained by the presence of initial gradients inherited in the material structure due to prior dislocation density, whose magnitudes are scaled by ℓ_o. On the contrary, the phenomenological expression assumed by Aifantis (e.g. see Tsagrakis and Aifantis, 2002; Konstantinidis and Aifantis, 2002) for the gradient coefficient $\propto p^{(1/m)-1}$ suggests that $\ell = 0$ when $p = 0$, and consequently it cannot explain the size effect on the yield point. On the other hand, k_1 determines the rate at which the size effect starts to diminish toward the conventional plasticity limit. From Figs. 10 and 11, it can be seen that k_1 depends on the work-hardening level in the material through the hardening exponent m, where k_1 for annealed iridium of $m = 8.9$ is bigger than that of annealed OFC of $m = 2$. Thus, k_1 increases as m decreases. Moreover, it is worth to mention that Pamin (1994) showed that the dependence of ℓ on the deformation level is necessary for the stability of the numerical implementation of the gradient-type theories.

Similar argument to that of the length-scale parameter can be concluded for the interaction coefficient β, such that the following evolution can be assumed:

$$\beta = \beta_o \exp(-k_2 p) \tag{59}$$

Figs. 10(b) and 11(b) show reasonable fits of the above expression to the calibrated values. It can be seen that the smaller the interaction coefficient β the more significant the interaction between SSDs and GNDs.

Clearly, numerical experiments of the indentation problem are required to verify those findings. Examples of two-diemensional verses three-diemensional indentation simulations can be found in a recent work by Muliana et al. (2002). In addition, numerical examples showing the effectiveness of the proposed equations in capturing the size dependent behavior as compared to the experimental results are required. Examples for such problems are micro-bending of thin beams, micro-torsion of thin wires, growth of microvoids, shear bands, and rate-dependent micro- and nano-indentation of thin films. However, this is not the subject of this study and will be addressed in a forthcoming work by the authors.

6. Conclusions

While such an increasing interest in gradient-enhanced theories can be understood in view of the aforementioned remedies they provide, actual experiments for the direct measurement of the material intrinsic length parameter introduced by the phenomenological gradient coefficients are lacking. When considering the microstructure with localization zones, gradient-dependent behavior is becoming important once the length-scale associated with the local deformation gradients becomes

sufficiently large when compared with the characteristic dimension of the system. It follows that such experiments could be difficult to design and interpret.

However, this paper provides an extended effort in this direction, where we discuss the issue of size effect and the analytical and experimental calibration of the strain gradient theory. A micromechanical model that assesses a nonlinear coupling between the statistically stored dislocations (SSDs) and the geometrically necessary dislocations (GNDs) is used in bridging the gap between the macromechanical plasticity and the micromechanical plasticity. Based on this proposed bridging an analytical expression is derived for the deformation-gradient-related intrinsic length-scale parameter ℓ in terms of measurable microstructural physical parameters. This is done through the use of the gradient theory to bring closer together the microstructural (described by the Taylor's hardening law) and continuum (described by the strain-hardening power law) descriptions of plasticity. As a result ℓ is defined in terms of the average distance between statistically stored dislocations L_S (characterizes the characteristic length of plasticity phenomenon), the Nye factor $\bar{r}$ (characterizes the microstructure dimension such as the grain size, grain boundary thickness, obstacle spacing and radius), the Schmidt's orientation factor $\bar{M}$ (characterizes the lattice rotation), the Burgers vector $\boldsymbol{b}$ (characterizes the displacement carried out by each dislocation), and the empirical constant α (characterizes the deviation from regular spatial arrangement of the SSD or GND populations).

In addition, the identification of the intrinsic material length scale from micro- and nano-indentation experiments is carried out. We showed, in particular, that gradient plasticity models can be used for the interpretation of size effect experiments in micro- and nano-indentation when using pyramidal and spherical indenters. In fact, the aforementioned gradient models are calibrated by fitting the corresponding length-scale parameter to the experimental data. Micro- and nano-indentation tests can thus be used for the experimental determination of the gradient length-scale parameter. The ISE in hardness experiments by pyramidal and spherical indenters is interpreted in such a way that the effective plastic strain should be constant. The ISE in spherical indentation can still be interpreted as an increase in hardness with decreasing indentation depth, or equivalently with increasing contact radius, as interpreted by the Nix and Gao (1998) model for pyramidal indentation. We have also been able to correlate reasonably successfully the nano- and micro-hardness from spherical and pyramidal indenters.

Materials with smaller ℓ are harder and require greater loads in order to create the same contact area, which dictates that the additional amount of hardening during deformation increases as ℓ increases. Thus, the hardest materials have the smallest values of ℓ. It is concluded that the size effect is more significant in annealed specimens than in cold-worked specimens. Therefore, the indentation size effect is expected to be influenced by both prior dislocations and the additional work hardening that occurs during indentation.

The Nix and Gao (1998) model and the Swadener et al. (2002a,b) model predictions deviate from the hardness experimental results, at small depths for the case of conical/pyramidal indenters and at small diameters for the case of spherical indenters. This deviation can be largely corrected by utilizing a proper value for the

interaction coefficient β, which compensates for the proper coupling between the SSDs and GNDs during indentation such that $\rho_T = \left[\rho_S^\beta + \rho_G^\beta\right]^{1/\beta}$. Therefore, the most likely impediment in the Nix and Gao (1998) model and Swadener et al. (2002a,b) model is the assumption that the SSD and GND densities are coupled in a linear sense, such that $\rho_T = \rho_S + \rho_G$; i.e. the ideal assumption of all the obstacles being equally strong and equally spaced along a straight or curved contacting line. However, the real situation in experiments suggests that the hardening law cannot be taken as a simple sum of the densities of SSDs and GNDs. Furthermore, it is shown that the smaller the interaction coefficient β, the more significant the interaction between SSDs and GNDs. In addition, the introduction of the interaction coefficient β into the mechanism-based plasticity constitutive models introduces an initial insight toward extending the strain-gradient plasticity theories to include size effects on the nano-scale.

The experimental results showed that the intrinsic material length-scale ℓ and the interaction coefficient β are not constant and evolve with deformation. Evolution laws have been proposed for ℓ and β in terms of the plastic strain. These laws suggest that the material ℓ and β decrease with increasing plastic strain. The effect of initial dislocation density that is nucleated during the specimen preparation is incorporated in these laws.

However, additional experimental measurements and numerical investigations are needed to fully verify the proposed procedure for the identification of the material intrinsic length-scale ℓ. Moreover, more studies are needed to identify the length-scale measures associated with the damage and fracture mechanisms. Therefore, no one yet may claim the final determination of the actual material intrinsic length-scale due to the lack of experimental procedures to do so and the lack of solid physical interpretations of the material intrinsic length-scale. Therefore, this is still an open question to researchers: What is the physical interpretation of the material intrinsic length-scale?

Acknowledgements

The authors are indebted to Professors Ted Belytschko and Elias C. Aifantis for helpful discussions during their independent visits to the Advanced Computational Solid Mechanics Laboratory at Louisiana State University in Baton Rouge, Louisiana.

References

Abu Al-Rub, R.K., Voyiadjis, G.Z. Determination of the material intrinsic length scale of gradient plasticity theory. Int. J. Multiscale Comp. Eng. (in press).

Adler, T.A., Dogan, O.N., 1997. Damage by indentation and single impact of hard particles on a high chromium white cast iron. Wear 203, 257–266.

Aifantis, E.C., 1984. On the microstructural origin of certain inelastic models. J. Eng. Mater. Technol. 106, 326–330.

Aifantis, E.C., 1987. The physics of plastic deformation. Int. J. Plasticity 3, 211–247.
Aifantis, E.C., 1999. Strain gradient interpretation of size effects. Int. J. Fract. 95, 299–314.
Aifantis, E.C., Oka, F., Yashima, A., Adachi, T., 1999. Instability of gradient dependent elastoviscoplasticity for Clay. Int. J. Numer. Analytical Meth. in Geomechanics 23 (10), 973–994.
Arsenlis, A., Parks, D.M., 1999. Crystallographic aspects of geometrically-necessary and statistically-stored dislocation density. Acta Mater. 47, 1597–1611.
Ashby, M.F., 1970. The deformation of plastically non-homogenous alloys. Philos. Mag. 21, 399–424.
Atkins, A.G., Tabor, D.T., 1965. Plastic indentation in metals with cones. J. Mech. Phys. Solids 13, 149–164.
Bammann, D.J., Aifantis, E.C., 1982. On a proposal for a continuum with microstructure. Acta Mech. 45, 91–121.
Bammann, D.J., Aifantis, E.C., 1987. A model for finite-deformation plasticity. Acta Mech. 69, 97–117.
Bammann, D.J., Mosher, D., Hughes, D.A., Moody, N.R., Dawson, P.R., 1999. Using Spatial Gradients to Model Localization Phenomena. Report SAND99-8588. Sandia National Laboratories, Albuquerque, New Mexico 87185 and Livermore, CA.
Bassani, J.L., 2001. Incompatibility and a simple gradient theory of plasticity. J. Mech. Phys. Solids 49, 1983–1996.
Begley, M.R., Hutchinson, J.W., 1998. The mechanics of size-dependent indentation. J. Mech. Phys. Solids 46, 2049–2068.
Bishop, J.F.W., Hill, R., 1951. A theoretical derivation of the plastic properties of a polycrystalline face-centered metal. Philos. Mag. 42, 1298–1307.
Biwa, S., Storakers, B., 1995. An analysis of fully plastic Brinell indentation. J. Mech. Phys. Solids 43, 1303–1333.
Busso, E.P., Meissonnier, F.T., O'Dowd, N.P., 2000. Gradient-dependent deformation of two-phase single crystals. J. Mech. Phys. Solids 48, 2333–2361.
Caceres, C.H., Poole, W.J., 2002. Hardness and flow strength in particulate metal matrix composites. Mater. Sci. Eng. A 332, 311–317.
Chiu, Y.L., Ngan, A.H.W., 2002. A TEM investigation on indentation plastic zones in Ni3Al(Cr,B) single crystals. Acta Mater. 50, 2677–2691.
Chen, S.H., Wang, T.C., 2002a. A new deformation theory with strain gradient effects. Int. J. Plasticity 18, 971–995.
Chen, S.H., Wang, T.C., 2002b. Interface crack problem with strain gradient effects. Int. J. Fracture 117, 25–37.
Columbus, D., Grujicic, M., 2002. A comparative discrete-dislocation/nonlocal crystal-plasticity analysis of plane-strain mode I fracture. Mater. Sci. Eng. A323, 386–402.
de Borst, R., Mühlhaus, H.-B., 1992. Gradient-dependent plasticity formulation and algorithmic aspects. Int. J. Numer. Methods Eng. 35, 521–539.
de Borst, R., Sluys, L.J., Mühlhaus, H.-B., Pamin, J., 1993. Fundamental issues in finite element analysis of localization of deformation. Eng. Computations 10, 99–121.
de Borst, R., Pamin, J., 1996. Some novel developments in finite element procedures for gradient-dependent plasticity. Int. J. Numer. Methods Eng. 39, 2477–2505.
De Guzman, M.S., Neubauer, G., Flinn, P., Nix, W.D., 1993. The role of indentation depth on the measured hardness of materials. Material Research Symposium Proceedings 308, 613–618.
Elmustafa, A.A., Stone, D.S., 2002. Indentation size effect in polycrystalline F.C.C metals. Acta Mater. 50, 3641–3650.
Elmustafa, A.A., Stone, D.S., 2003. Nanoindentation and the indentation size effect: kinetics of deformation and strain gradient plasticity. J. Mech. Phys. Solids 51, 357–381.
Eringen, A.C., Edelen, D.G.B., 1972. On non-local elasticity. Int. J. Eng. Sci. 10, 233–248.
Field, J.S., Swain, M., 1993. A simple predictive model for spherical indentation. J. Mater. Res. 8, 297–306.
Fleck, N.A., Hutchinson, J.W., 1993. A phenomenological theory for strain gradient effects in plasticity. J. Mech. Phys. Solids 41, 1825–1857.

Fleck, N.A., Muller, G.M., Ashby, M.F., Hutchinson, J.W., 1994. Strain gradient plasticity: theory and experiment. Acta Metall. Mater. 42, 475–487.
Fleck, N.A., Hutchinson, J.W., 1997. Strain gradient plasticity. Adv. Appl. Mech. 33, 295–361.
Fleck, N.A., Hutchinson, J.W., 2001. A reformulation of strain gradient plasticity. J. Mech. Phys. Solids 49, 2245–2271.
Gao, H., Huang, Y., Nix, W.D., Hutchinson, J.W., 1999a. Mechanism-based strain gradient plasticity—I. Theory. J. Mech. Phys. Solids 47, 1239–1263.
Gao, H., Huang, Y., Nix, W.D., 1999b. Modeling plasticity at the micrometer scale. Naturwissenschaften 86, 507–515.
Gao, H., Huang, Y., 2001. Taylor-based nonlocal theory of plasticity. Int. J. Solids Struct. 38, 2615–2637.
Gao, H., Huang, Y., 2003. Geometrically necessary dislocation and size-dependent plasticity. Scripta Mater. 48, 113–118.
Gerberich, W.W., Tymiak, N.I., Grunlan, J.C., Horstemeyer, M.F., Baskes, M.I., 2002. Interpretation of indentation size effects. ASME Trans., J. Appl. Mech. 69, 433–442.
Gracio, J.J., 1994. The double effect of grain size on the work-hardening behavior of polycrystalline copper. Scripta Metall. Mater. 31, 487–489.
Guo, Y., Huang, Y., Gao, H., Zhuang, Z., Hwang, K.C., 2001. Taylor-based nonlocal theory of plasticity: numerical studies of the micro-indentation experiments and crack tip fields. Int. J. Solids Struct. 38, 7447–7460.
Gurtin, M.E., 2003. On a framework for small-deformation viscoplasticity: free energy, microforces, strain gradients. Int. J. Plasticity 19, 47–90.
Hill, R., 1950. Mathematical Theory of Plasticity. Oxford University Press, Oxford.
Hill, R., Storakers, B., Zdunek, A.B., 1989. A theoretical study of the Brinell hardness test. Proc. Royal Soc. London Series A Mathematical Physical and Engineering Sciences 423 (1865), 301–330.
Hirsch, P.B. (Ed.), 1975. The Physics of Metals, Vol. 2. Cambridge University Press, Cambridge.
Huang, Y., Gao, H., Nix, W.D., Hutchinson, J.W., 2000a. Mechanism-based strain gradient plasticity—II analysis. J. Mech. Phys. Solids 48, 99–128.
Huang, Y., Xue, Z., Gao, H., Xia, Z.C., 2000b. A study of micro-indentation hardness tests by mechanism-based strain gradient plasticity. J. Mater. Res. 15, 1786–1796.
Huber, N., Tsakmakis, Ch., 1999. Determination of constitutive properties from spherical indentation data using neural networks. Part II: plasticity with nonlinear isotropic and kinematic hardening. J. Mech. Phys. Solids 47, 1589–1607.
Huber, N., Nix, W.D., Gao, H., 2002. Identification of elastic-plastic material parameters from pyramidal indentation of thin films. Proc. Royal Soc. London Series A 458 (2023), 1593–1620.
Hwang, K.C., Jiang, H., Huang, Y., Gao, H., Hu, N., 2002. A finite deformation theory of strain gradient plasticity. J. Mech. Phys. Solids 50, 81–99.
Hwang, K.C., Jiang, H., Huang, Y., Gao, H., 2003. Finite deformation analysis of mechanism-based strain gradient plasticity: torsion and crack tip field. Int. J. Plasticity 19, 235–251.
Imamura, S., Stao, Y., 1986. The size effect on yielding of a mild steel strip with a hole under tension. Trans. Jpn. Soc. Mech. Eng. Ser. A 52, 1440–1444 (in Japanese).
Johnson, K.L., 1970. The correltion of indentation experiments. J. Mech. Phys. Solids 18, 115–126.
Johnson, K.L., 1985. Contact Mechanics. Cambridge University Press, Cambridge.
Kiser, M.T., Zok, F.W., Wilkinson, D.S., 1996. Plastic flow and fracture of a particulate metal matrix composite. Acta Mater. 44, 3465–3476.
Kroner, E., 1962. Dislocations and continuum mechanics. Appl. Mech. Rev. 15, 599–606.
Kroner, E., 1967. Elasticity theory of materials with long range cohesive forces. Int. J. Solids Struct. 24, 581–597.
Kocks, U.F., 1966. A statistical theory of flow stress and work hardening. Philos. Mag. 13, 541.
Kocks, U.F., 1970. The relation between polycrystal deformation and single-crystal deformation. Metall. Trans. 1, 1121–1141.
Kocks, U.F., Argon, A.S., Ashby, M.F., 1975. Thermodynamics and Kinetics of Slip. Progress in Materials Science, Vol. 19. Pergamon Press, Oxford.

Konstantinidis, A.A., Aifantis, E.C., 2002. Recent developments in gradient plasticity—part II: plastic heterogeneity and wavelets. ASME Trans., J. Eng. Mater. Technol. 124, 358–364.
Kucharski, S., Mroz, Z., 2001. Identification of plastic hardening parameters of metals from spherical indentation tests. Mater. Sci. Eng. A318, 65–76.
Kuhl, E., Ramm, E., de Borst, R., 2000. An anisotropic gradient damage model for quasi-brittle materials. Comput. Methods Appl. Mech. Eng. 183, 87–103.
Lasry, D., Belytschko, T., 1988. Localization limiters in transient problems. Int. J. Solids Struct. 24, 581–597.
Lim, Y.Y., Bushby, A.J., Chaudhri, Y.Y., 1998. Nano and macro indentation studies of polycrystalline copper using spherical indenters. Mater. Res. Soc. Symp. Proc. 522, 145–150.
Lim, Y.Y., Chaudhri, Y.Y., 1999. The effect of the indenter load on the nanohardness of ductile metals: an experimental study of polycrystalline work-hardened and annealed oxygen-free copper. Philos. Mag. A 79 (12), 2979–3000.
Lloyd, D.J., 1994. Particle reinforced aluminum and magnesium matrix composites. Int. Mater. Rev. 39, 1–23.
Ma, Q., Clarke, D.R., 1995. Size dependent hardness in silver single crystals. J. Mater. Res. 10, 853–863.
McElhaney, K.W., Valssak, J.J., Nix, W.D., 1998. Determination of indenter tip geometry and indentation contact area for depth sensing indentation experiments. J. Mater. Res. 13, 1300–1306.
McClintock, F.A., Argon, A.S., 1966. Mechanical Behavior of Materials. Addison-Wesley, Reading, MA.
Mühlhaus, H.B., Aifantis, E.C., 1991. A variational principle for gradient principle. Int. J. Solids Struct. 28, 845–857.
Muliana, A., Steward, R., Haj-Ali, R., Saxena, A., 2002. Artificial neural network and finite element modeling of nanoindentation tests. Metall. Mater. Trans. A 33, 1939–1947.
Nan, C.-W., Clarke, D.R., 1996. The influence of particle size and particle fracture on the elastic/plastic deformation of metal matrix composites. Acta Mater. 44, 3801–3811.
Nix, W.D., Gao, H., 1998. Indentation size effects in crystalline materials: a law for strain gradient plasticity. J. Mech. Phys. Solids 46, 411–425.
Oka, F., Yashima, A., Sawada, K., Aifantis, E.C., 2000. Instability of gradient-dependent elastoviscoplastic model for clay and strain localization analysis. Computer Methods in Appl. Mech. Eng. 183, 67–86.
Oliver, W.C., Pharr, G.M., 1992. An improved technique for determining hardness and elastic modulus using load and displacement sensing indentation experiments. J. Mater. Res. 7, 1564–1583.
Pamin, J., 1994. Gradeitn-Dependent Plasticity in Numerical Simulation of Localization Phenomena. Dissertation, Delft University of Technology.
Peerlings, R.H.J., de Borst, R., Brekelmans, W.A.M., de Vree, J.H.P., 1996. Gradient enhanced damage for quasi-brittle materials. Int. J. Numer. Methods Eng. 39, 3391–3403.
Pijaudier-Cabot, T.G.P., Bazant, Z.P., 1987. Nonlocal damage theory. ASCE J. Eng. Mech. 113, 1512–1533.
Poole, W.J., Ashby, M.F., Fleck, N.A., 1996. Micro-hardness of annealed and work-hardened copper polycrystals. Scripta Mater. 34, 559–564.
Qiu, X., Huang, Y., Nix, W.D., Hwang, K.C., Gao, H., 2001. Effect of intrinsic lattice resistance in strain gradient plasticity. Acta Mater. 49, 3949–3958.
Rhee, M., Hirth, J.P., Zbib, H.M., 1994a. A superdislocation model for the strengthening of metal matrix composites and the initiation and propagation of shear bands. Acta Metall. Mater. 42, 2645–2655.
Rhee, M., Hirth, J.P., Zbib, H.M., 1994b. On the bowed out tilt wall model of flow stress and size effects in metal matrix composites. Scripta Metall. Mater. 31, 1321–1324.
Robinson, W.H., Truman, S.D., 1977. Stress-strain curve for aluminum from a continuous indentation test. J. Mater. Sci. 12, 1961–1965.
Saha, R., Xue, Z., Huang, Y., Nix, W.D., 2001. Indentation of a soft metal film on a hard substrate: strain gradient hardening effects. J. Mech. Phys. Solids 49, 1997–2014.
Saczuk, J., Hackl, K., Stumpf, H., 2003. Rate theory of nonlocal gradient damage-gradient viscoinelasticity. Int. J. Plasticity 19, 675–706.
Shu, J.Y., Fleck, N.A., 1998. The prediction of a size effect in micro-indentation. Int. J. Solids Struct. 35, 1363–1383.
Shu, J.Y., Fleck, N.A., 1999. Strain gradient crystal plasticity: size dependent deformation in bicrystals. J. Mech. Phys. Solids 47, 297–324.

Shu, J.Y., Barrlow, C.Y., 2000. Strain gradient effects on microscopic strain field in a metal matrix composite. Int. J. Plasticity 16, 563–591.

Shen, Y.-L., Chawla, N., 2001. On the correlation between hardness and tensile strength in particle reinforced metal matrix composites. Mater. Sci. Eng. A 297, 44–47.

Stolken, J.S., Evans, A.G., 1998. A microbend test method for measuring the plasticity length-scale. Acta Mater. 46, 5109–5115.

Stelmashenko, N.A., Walls, M.G., Brown, L.M., Milman, Y.V., 1993. Microindentation on W and Mo oriented single crystals: an STM study. Acta Metall. Mater. 41, 2855–2865.

Swadener, J.G., George, E.P., Pharr, G.M., 2002a. The correlation of the indentation size effect measured with indenters of various shapes. J. Mech. Phys. Solids 50, 681–694.

Swadener, J.G., Misra, A., Hoagland, R.G., Nastasi, M., 2002b. A mechanistic description of combined hardening and size effects. Scripta Mater. 47, 343–348.

Taylor, G.I., 1938. Plastic strain in metals. J. Inst. Metals 62, 307–324.

Tabor, D., 1951. The Hardness of Metals. Clarendon Press, Oxford.

Tabor, D., 1996. Indentation hardness: fifty years on, a personal view. Philos. Mag. A 74 (5), 1207–1212.

Tangena, A.G., Hurkx, G.A.M., 1986. Determination of stress–strain curves of thin layers using indentation tests. ASME J. Eng. Mater. Technol. 108, 230–232.

Taylor, M.B., Zbib, H.M., Khaleel, M.A., 2002. Damage and size effect during superplastic deformation. Int. J. Plasticity 18, 415–442.

Tsagrakis, I., Aifantis, E.C., 2002. Recent developments in gradient plasticity—part I: formulation and size effects. ASME Trans., J. Eng. Mat. Technol. 124, 352–357.

Tymiak, N.I., Kramer, D.E., Bahr, D.F., Wyrobek, T.J., Gerberich, W.W., 2001. Plastic strain and strain gradients at very small indentation depths. Acta Mater. 49, 1021–1034.

Voyiadjis, G.Z., Deliktas, B., Aifantis, E.C., 2001. Multiscale analysis of multiple damage mechanics coupled with inelastic behavior of composite materials. J. Eng. Mech. 127, 636–645.

Voyiadjis, G.Z., Dorgan, R.J., 2001. Gradient formulation in coupled damage-plasticity. Archives of Mech. 53, 565–597.

Voyiadjis, G.Z., Abu Al-Rub, R.K., Palazotto, A.N., 2003a. Non-local coupling of viscoplasticity and anisotropic viscodamage for impact problems using the gradient theory. Archives of Mechanics 55, 39–89.

Voyiadjis, G.Z., Abu Al-Rub, R.K., Palazotto, A.N. Thermodynamic formulations for non-local coupling of viscoplasticity and anisotropic viscodamage for dynamic localization problems using gradient theory. Int. J. Plasticity (in press).

Wang, W.M., Askes, H., Sluys, L.J., 1998. Gradient viscoplastic modeling of material instabilities in metals. Metals and Materials-Korea 4, 537–542.

Wang, W., Huang, Y., Hsia, K.J., Hu, K.X., Chandra, A., 2003. A study of microbend test by strain gradient plasticity. Int. J. Plasticity 19, 365–382.

Xue, Z., Huang, Y., Li, M., 2002a. Particle size effect in metallic materials: a study by the theory of mechanism-based strain gradient plasticity. Acta Mater. 50, 149–160.

Xue, Z., Huang, Y., Hwang, K.C., Li, M., 2002b. The influence of indenter tip radius on the micro-indentation hardness. ASME J. Eng. Mater. Technol. 124, 371–379.

Xue, Z., Saif, M.T.A., Huang, Y., 2002c. The strain gradient effect in microelectromechanical systems (MEMS). J. Microelectromechanical Systems 11, 27–35.

Yuan, H., Chen, J., 2001. Identification of the intrinsic material length in gradient plasticity theory from micro-indentation tests. Int. J. Solids Struct. 38, 8171–8187.

Zaiser, M., Aifantis, E.C., 2003. Geometrically necessary dislocations and strain gradient plasticity—a dislocation dynamics point of view. Scripta Mater. 48, 133–139.

Zbib, H.M., Aifantis, E.C., 1988. On the localization and postlocalization behavior of plastic deformation, I, II, III. Res. Mechanica 23, 261–277, 279–292, 293–305.

Zhu, H.T., Zbib, H.M., 1995. Flow strength and size effect of an Al–Si–Mg composite model system under multiaxial loading. Scripta Metall. Mater. 32, 1895–1902.

Zhu, H.T., Zbib, H.M., Aifantis, E.C., 1997. Strain gradients and continuum modeling of size effect in metal matrix composites. Acta Mech. 121, 165–176.